Chapter 10

Isotropic Migration Velocity Analysis

Velocity analysis is one of the most important aspects of imaging seismic data. Regardless of whether the project is a prestack time or depth migration, finding an Earth model that produces the best possible image is seldom easy. What we know today is that finding the *optimum* isotropic velocity is directly related to the experience of the analyst, the quality of the migration tools at his or her disposal, and, of course, the quality of the seismic data itself.

Almost all velocity analysis done today is what is normally referred to as migration velocity analysis (MVA), and is usually based on some form of semblance calculation and picking. This works reasonably well so long as the Earth model is isotropic, but when the subsurface is anisotropic, it falls far short of producing reasonable estimates of the totality of parameters defining the anisotropic world. Moreover, as we saw the estimated velocity may produce a high quality image with excellent lateral positioning, but depth conversions will be inaccurate. In this case, the analyst must have proper tools for improving the number and accuracy of the parameters in the ultimate Earth model.

Almost nothing can be done about the seismic data from which the required Earth model parameters must be estimated. There are certain simple preprocessing steps that can at least reduce the possibility of limiting the quality of the final image. Some good and bad data preparation practices are summarized in the following list:

- Deconvolution is good, provided that it enhances low frequency content
- Removing low frequencies is bad
  - Velocity analysis requires many low but not so many high frequencies
  - Migration basically trades horizontal wavenumber for vertical wavenumbers
  - Migrate the data first to assess the need for low frequency removal

- Two dimensional linear noise reduction may reduce dips
  - FK or fan filters should be avoided unless absolutely necessary
  - Prestack migration usually images linear noise to a point or off the section

- Multiple suppression can be a necessary
  - SRME/Inverse Scattering is the optimum choice
  - Parabolic methods should be used with care

- Migration from topography should always be a priority
  - Sea floor topography is the same as topography
  - Refraction statics should really be refraction tomography

In the author's mind, there are four basic approaches to MVA.

- The first approach is what we will call *short-spread-semblance-based* velocity analysis. This velocity analysis is based on a short enough spread to avoid anisotropic effects and essentially provides what we have referred to as the NMO velocity. It is useful for both compressional and, when available, shear data. Typically, it does not consider issues related to any form of anisotropy. It can be completed with or without horizons. This approach has been the workhorse of MVA for many years.

- The second approach continues the use of the *short spread* approach, but adds residual tomography to the mix. When the short-spread analysis methodology is considered to have run its course, residual picks are used in a tomographic inversion to produce a refined update. Tomography sometimes suffers from a lack of redundancy that precludes its usefulness. It may also have problems due to short spread limitations. In the traditional formulation, it may not have sufficiently wide incidence angles to be effective. In some cases, the tomographic inversion can be used to estimate simple anisotropic parameters, but this does not appear to be routine.

- The third velocity analysis approach relaxes the short-spread assumptions, uses all the data, and incorporates well information directly into the mix. This combination of techniques requires the availability of additional data, usually in the form of shear measurements, but some form of subsurface information is a must. Subsurface knowledge can be empirical, rather then from a drill bit, but it is a must. This approach requires much more interpretive input than the other two. Perhaps its chief drawback is its continued dependence on semblance style picking.

- The fourth, and definitely least used and understood methodology, is what we will call *full-waveform inversion*. This is what we might refer to as a hands-off method. We formulate the problem in a purely mathematical sense and let a super computer do all the work. While this approach, for the most part, has failed miserably in the past, there are beginning to be indications that with the right data, full-waveform

inversion may eventually become a useful tool. What is becoming clear is that for full-waveform processing to become a useful technology, the industry must begin to acquire much lower frequency and more densely sampled data. In addition, computation power will have to increase several orders of magnitude, and the cost of compute cycles will also have to decrease significantly as well.

Migration Velocity Analysis Geometry

Figure 10-1 graphically represents the basic idea behind migration velocity analysis. Velocity analysis after migration estimates the velocity along the vertical from the surface to the migrated output point. Of course, because it assumes that the source and receiver are coincident, one cannot base a velocity analysis approach on this kind of concept alone.

Figure 10-1. Migration velocity analysis geometry

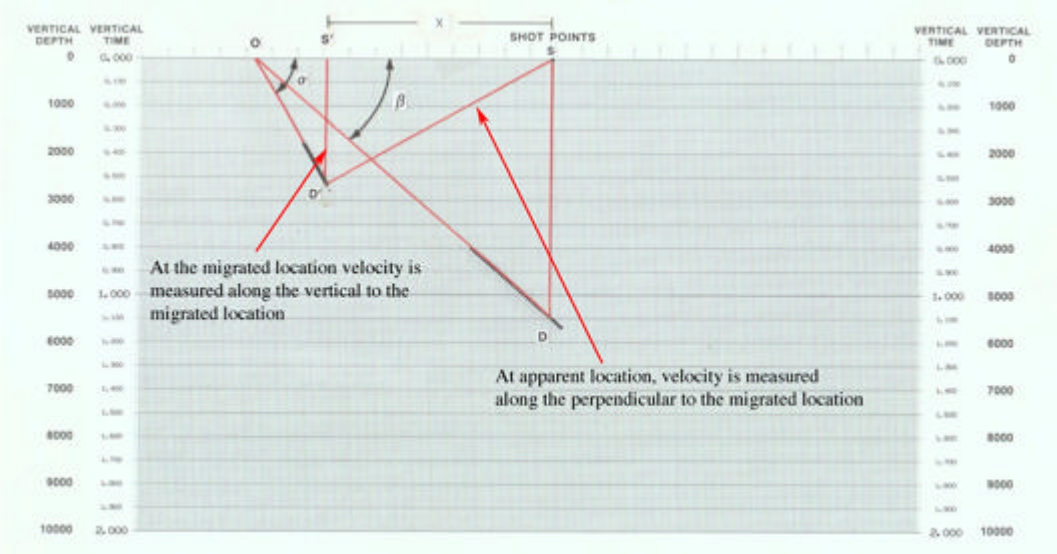

Developing a reasonable approach to velocity analysis requires that we have redundant data and that we exploit this redundancy in order to provide velocity estimates. Figure 10-2 illustrates the geometry in the case of non-zero offset from a ray-based modeling perspective. We see that the recorded data, in yellow, is placed below the surface midpoint. The red and green rays illustrate the paths taken by the illuminating energy. After migration, the yellow apparent event is now places at its true location below the vertical black image ray. Migration has moved the source and receiver locations directly above the correct location. Thus, after migration, source and receiver locations are lost. We can maintain redundancy by migrating common-offset sections and hopefully develop velocity analysis approaches that are applied after migration. Our goal is to provide velocity analysis methodologies that exploit residual redundancy to refine initial velocity estimates.

Figure 10-2. Migration velocity analysis geometry

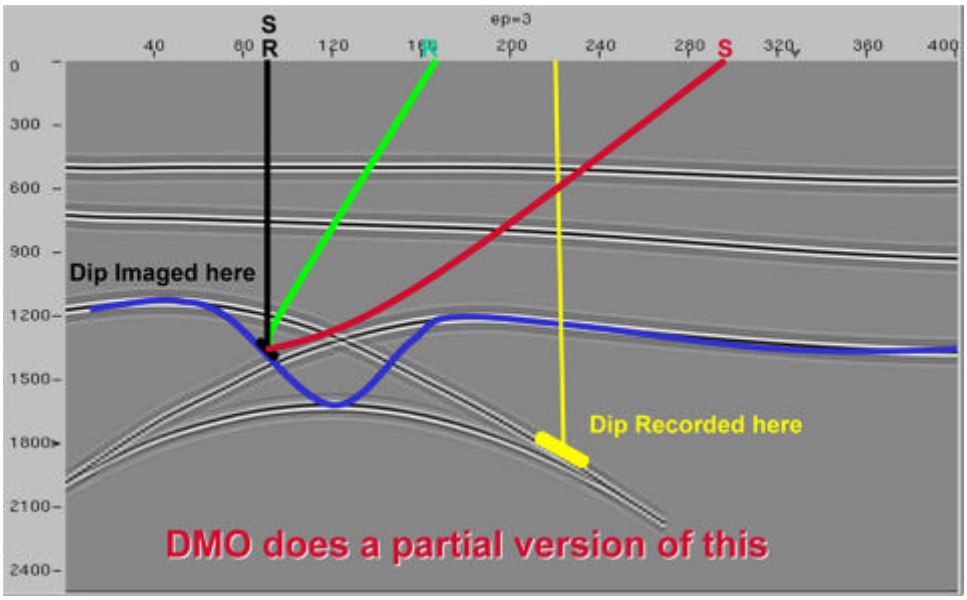

Constant Velocity Migration Velocity Analysis

An early approach to pre-stack-time migration velocity analysis is illustrated in Figure 10-3. The approach was popularized by Paul Fowler at the Stanford Exploration Project and later at Western Geophysical in Houston, Texas. In part (a) we see the general idea is to perform many constant velocity pre-stack time migrations and collect the resulting information into a cube with axis for time, CDP, and velocity. Each fixed CDP (y in this case) is then analyzed to select the optimum velocity at that location. Figure 10-3b compares more traditional stacking velocity and DMO based approaches to the one described by (a). The general conclusion is that the constant velocity approach is somewhat better than the other two.

Figure 10-3. Migration velocity analysis geometry

(a). Constant velocity PSTM gathers

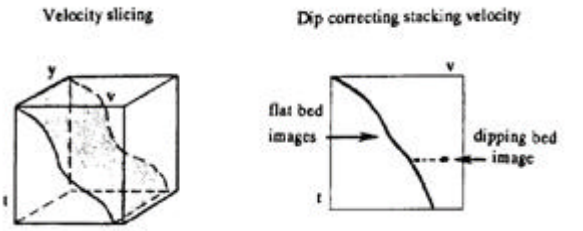

FIG. 1. (a) Extracting a stacked section corresponding to a specified velocity function by "slicing" through the three-dimensional velocity-midpoint-time data cube. (b) Correction of high stacking velocities due to dip, as seen in a (*v,t*) velocity panel.

(b). Constant velocity PSTM image comparisons

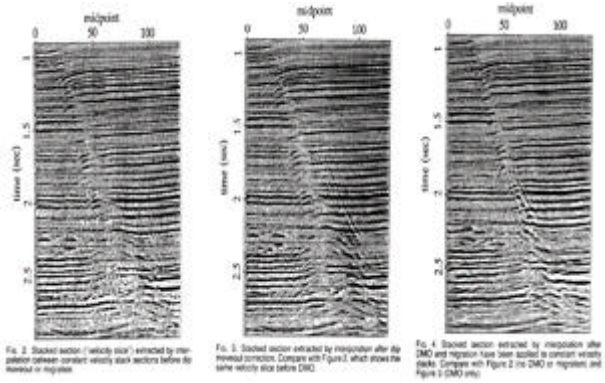

Velocity Independent Migration Velocity Analysis

Another early approach to PSTM velocity analysis is illustrated in Figure 10-4. The important issue with regard to Figure 10-4 is that we can apply this migration algorithm without knowledge of the velocity. Once applied, a detailed analysis can then be performed to determine the velocity that best flattens the gathers and produces the best image. It is very important to note that this approach produces velocities that are obtained at the migrated positions. Thus, the requirement of Figure 10-1 is met: The velocity is at the migrated or *vertical* position where it is actually needed.

Figure 10-4. Imaging without the velocity

(a). Midpoint and offset sorts of a point source

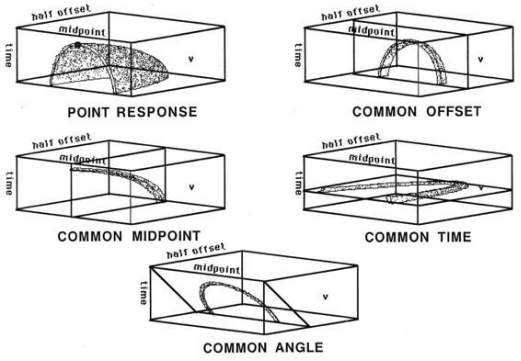

(b). Dip independent constant velocity imaging

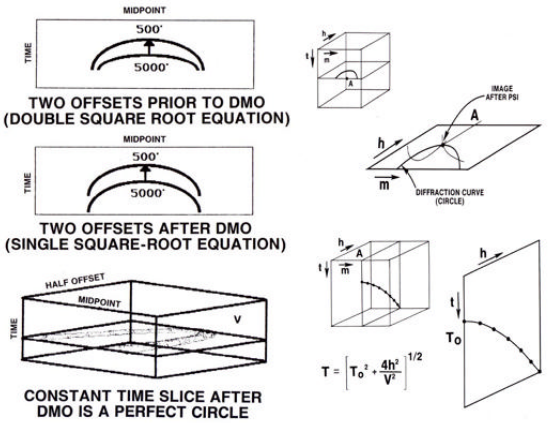

There are many variations of this approach. One, due to John C. Bancroft at the University of Calgary and his colleagues, is called Equivalent Offset Migration, but, except for the fact that it is not velocity independent, it is essentially equivalent to what is described here.

Because this so-called velocity-independent approach is predicated on a constant velocity assumption, it and the Fowler method are to a large extent identical in the kinds of velocity models they produce. They are easily extended to 3D and can form the basis for automatic estimation of initial velocity fields, but they are for the most part PSTM methodologies. As we will see, the semblance-based approach in item 2 on page 254 has a natural extension to depth migration based migration velocity analysis (MVA) methods.

Migrated Common Image Gathers

There are at least four types of common image gathers that are suited to velocity analysis after migration. You can probably find many more, but for our purposes, the four we explain in this section will suffice.

Common Offset Migrated Velocity Analysis

The best known of these methods is Kirchhoff-based and produces migrated trace ensembles based on migrating common input offset volumes. The advantage of the Kirchhoff method is that we need not output every CIG during the migration process. Indeed, we can focus on local areas, coarse grids, target lines, or just about any form of output to use in the velocity analysis stage. The assumptions of this method are best summarized in Figure 10-5. It is clear that offset information has been transfered to the output point by simply shifting the source and receiver locations so that the new mid-point is the current image or output location. Figure 10-6(a) provides the scheme by which such offset gathers are produced.

Figure 10-5. Migration velocity analysis geometry

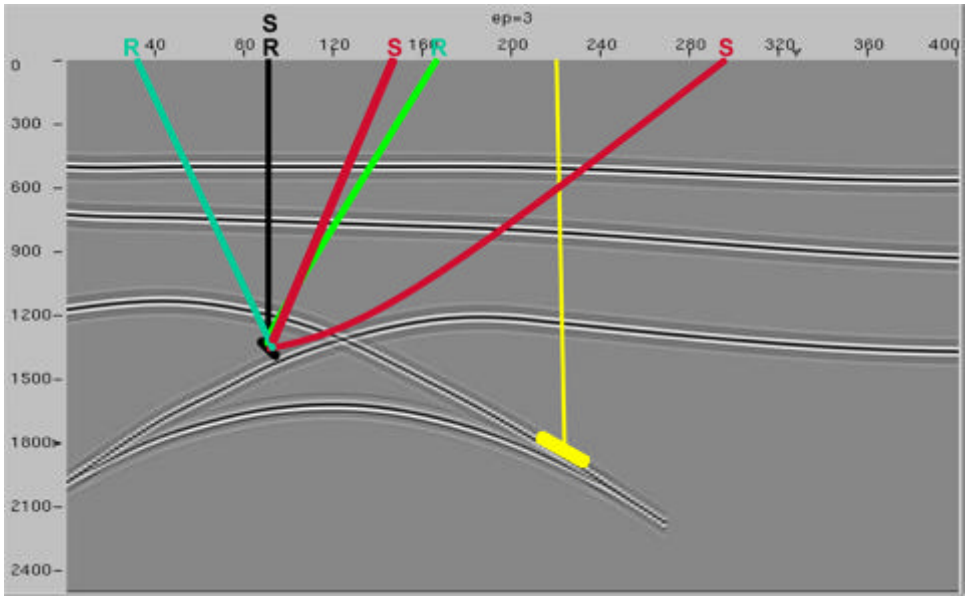

Figure 10-6(a) demonstrates the application of Kirchhoff migration on an offset-by-offset basis. Separating the output data by input offset means that we quite naturally produce input-offset gathers at each surface-defined image point. Such gathers are easily understood by processors used to thinking in stacking velocity analysis terms.

The Kirchhoff method is difficult but not impossible to extend to shot migration approaches. In the case of shot migrations, it is quite easy to produce three gather styles: Angle gathers, shot-profile migrated image gathers, and depth-focusing gathers. All three are based on time-shift, offset-shift, or vertical-shift gathers produced during the prestack migration stage. As we pointed out in the prestack algorithm chapter, these gathers carry information directly related to whether or not the velocity at any give point in the subsurface is accurate or not.

Common Angle Migration Velocity Analysis

Perhaps the best way to understand angle gathers is visualized in Figure 10-6(b). From a ray-theoretic point of view, we are holding the opening angle (or double the incidence angle) constant and producing output volumes parameterized by the opening angles. Relatively complex mathematics allows us to compute these gathers after the completion of the migration process but before removal of recording redundancy. An advantage of these gather styles is that they can convey considerable information about the kinds of analysis limits we might encounter prior to encountering them.

Figure 10-6. The three basic velocity analysis gathers

(a). Common-offset based Common Image Gathers (CIG)

(b). Common-angle gathers (CAG)

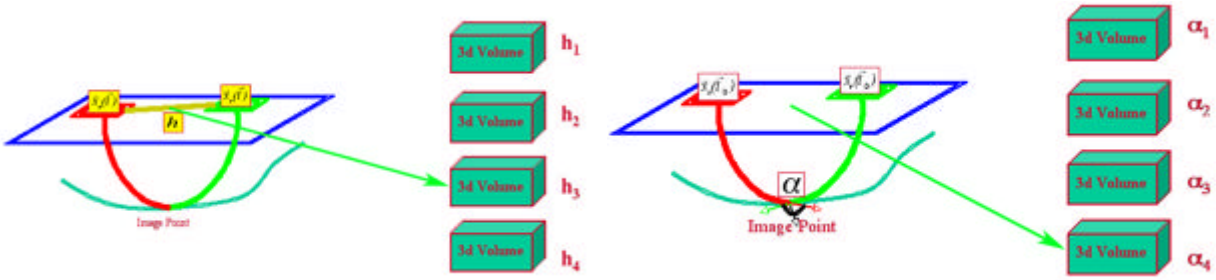

(c). Shot-profile migrated common image gathers (SMIGs)

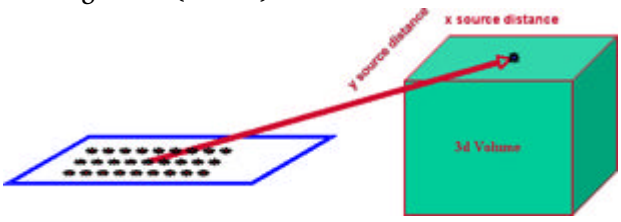

The production of common angle gathers as shown in Figure 10-6(b) is essentially the same as the process in (a). The difference is that, instead of holding the input offset constant, the process fixes the subsurface incidence angle to produce common angle gathers. Common angle gathers are certainly worth utilizing, but are somewhat difficult to use and are a bit costly to generate.

Shot Profile Migrated Image Gather Migration Velocity Analysis

Producing image gathers of any useful form from a set of shot-profile images hinges directly on the observation that after migration, the source and receiver are coincident. This fact is independent of migration algorithm—it does not matter whether the input data are migrated offset by offset, shot by shot, or common midpoint by common midpoint. When we migrate offset-by-offset and form common offset gathers based on the original input offset, we are assuming that the image point is directly below the midpoint of imaginary sources and receivers at half the offset distance on either side of the midpoint. Note that this also strongly implies that the migrated data have a fixed and common azimuth. We also expect this to produce precise velocity estimates.

Figure 10-6(c) represents what we call *shot-profile-common-image gathers*. A SMIG consists of all shots where the aperture contains a given fixed output image point. The migrated offset in this case is exactly half the distance from the image point to the source location for each trace in the gather. The reason for using half the distance will become clear in subsequent discussions. It is worth noting that SMIGs are not common receiver gathers. Since the fixed point is an output surface image location, they are true image gathers. They can also be three dimensional.

In the case of SMIGs, as depicted in Figure 10-7(a) and (b), we assume that, after the migration, the image point is directly below a source and receiver, and that it is again separated by a half offset, except that in this instance, the offset is the distance between the image point and the source. It is important to observe that these gathers are not common receiver gathers since surface receiver information is no longer available after migration.

Figure 10-7. Shot-profile-migrated common image gathers (SMIGs)

(a). Graphic explanation shot-profile-migrated common image gathers are formed

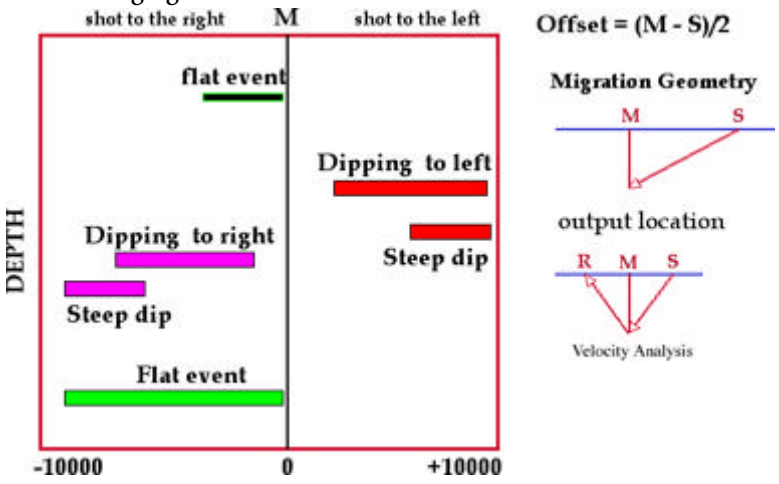

(b). Example shot-profile-migrated common image gather

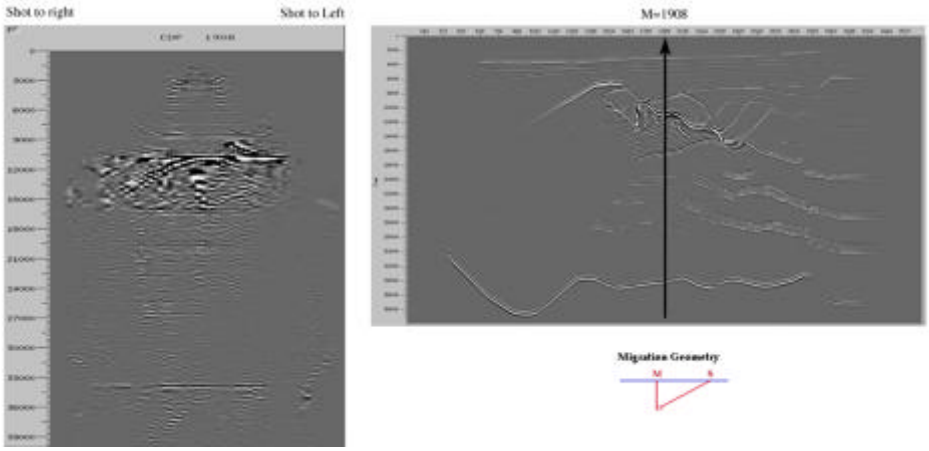

Depth Focusing Migration Velocity Analysis

Depth focusing analysis gathers are essentially the information used to produce angle gathers. They can be formed from either the time-shift or the offset-shift imaging conditions, or even vertical depth-shift imaging conditions described in the section on shot-profile migration.

Figure 10-8 illustrates the process. Part (a) is a cartoon of forward shot propagation, while (b) is a similar figure for the backward propagation of the receiver data. By shifting the arrivals vertically, laterally or temporally, we produce information that can be analyzed to find the maximum energy in the arrival.

Figure 10-8. Key Elements of depth focusing analysis.

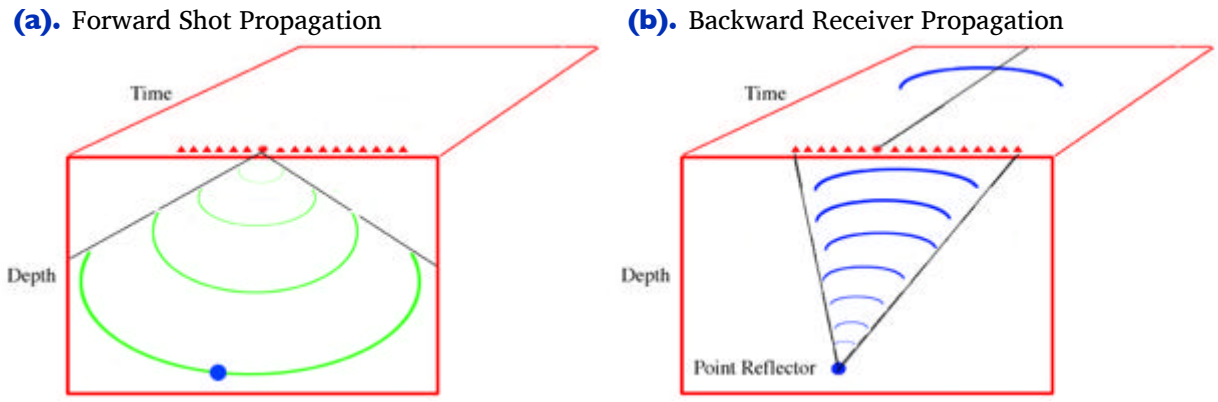

Figure 10-9(a) shows gathers produced by a time-shift imaging condition. The horizontal axis in this figure is depth and the vertical axis is time. Part (b) shows the relative depth shift from a fixed position. If the velocities at each depth are correct. the maximum energy arrivals will line up at zero time.

Figure 10-9. Depth Focusing Analysis. (After S. Mackay and R. Abma)

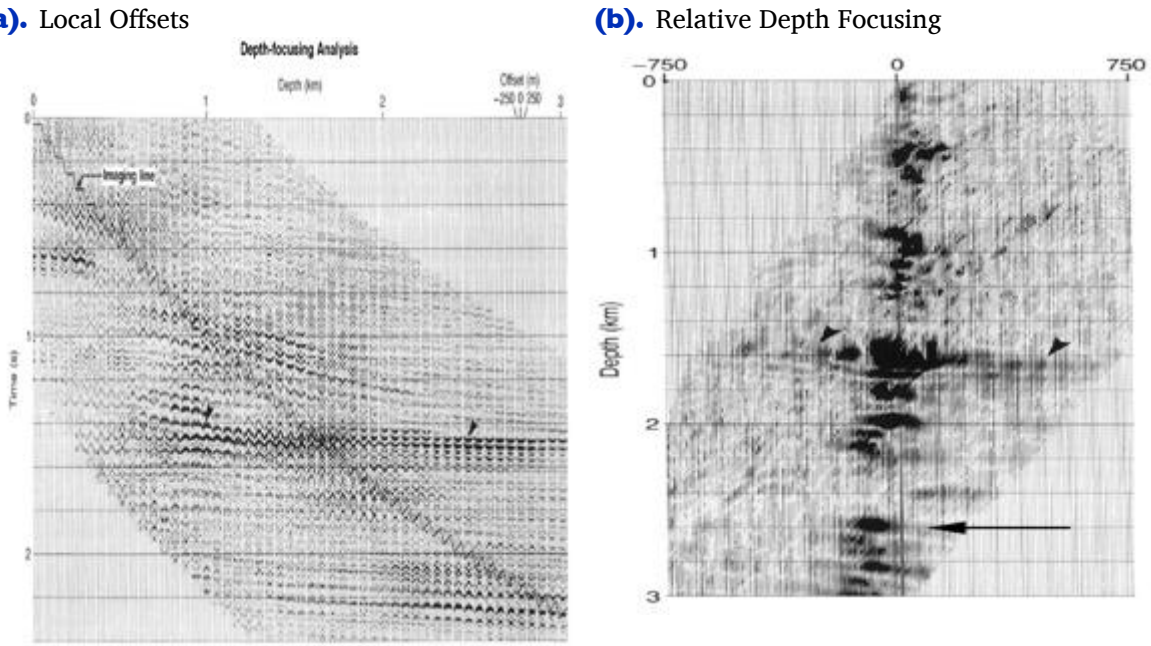

Semblance-Based Isotropic MVA on CIGs, CAGs, and SMIGs

Figure 10-10(a) shows common input offset image gathers generated by migrating each input sorted offset with a most energetic arrival Kirchhoff algorithm. Figure 10-10(b) shows common azimuth generated common angle gathers and associated common angle semblance panels. The angles range from 0 to 60 degrees in increments of 2 degrees.

Figure 10-10. Common input offset and common angle gathers.

(a). Input offset Kirchhoff common image gathers

(b). Input offset common azimuth common angle gathers

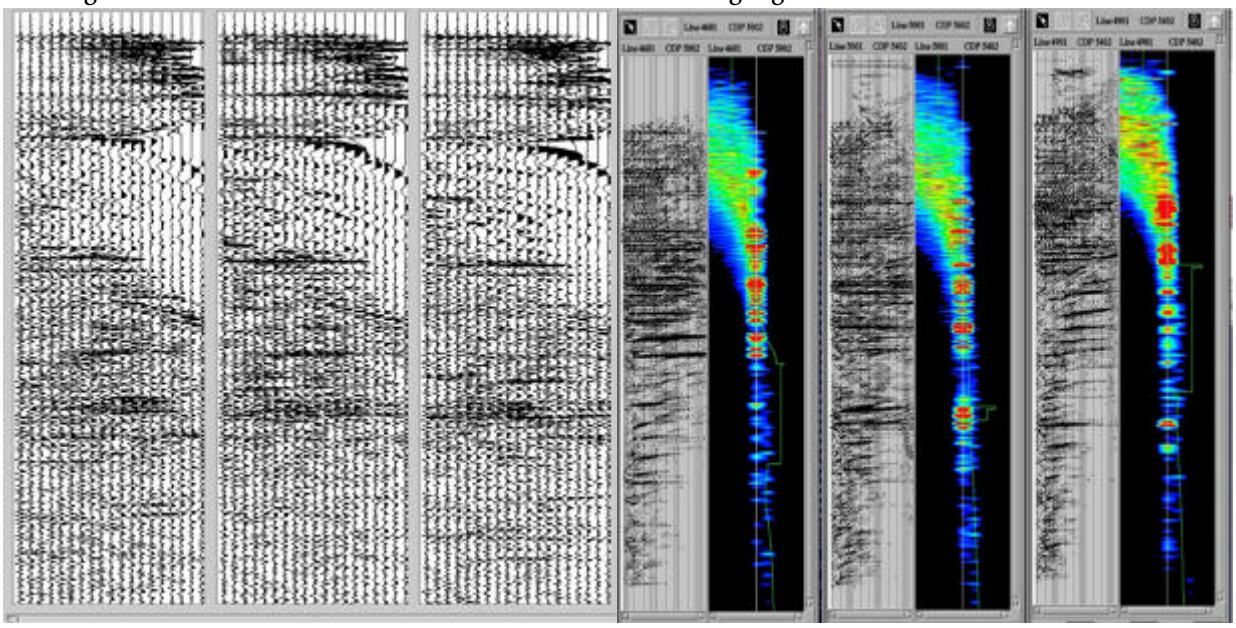

Figure 10-11(a) visualizes the kind of information angle gathers provide in sediments as compared to subsalt settings. In (a), the general loss of angle information is gradual as depth increases. In contrast, (b) shows that the loss of angle information below salt (or any high velocity anomaly) is quite dramatic. This is one reason angle gathers might be preferred over other forms of velocity analysis.

Figure 10-11. Common angle gathers. Sediments versus Salt

(a). Angle Gathers in Sediments **(b).** Angle Gathers below Salt

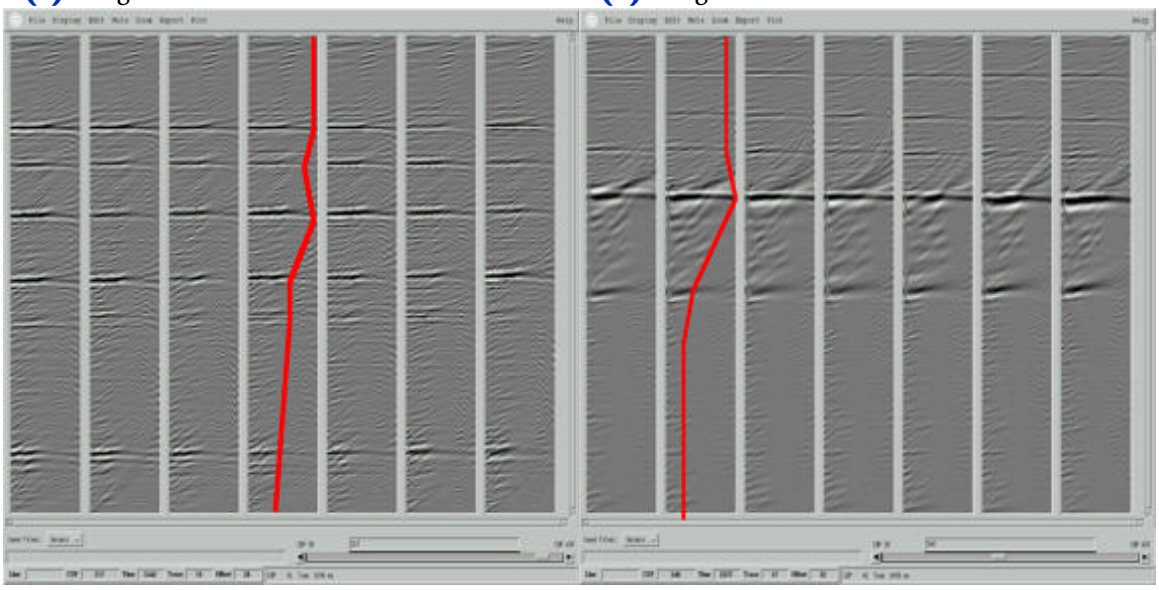

The velocity analysis/inversion formulas for estimating velocity models from either offset or angle gathers are shown in Figure 10-12. Note that the difference occurs because, in the old case, the method estimates velocity without any knowledge of the velocity used in the migration process, while in the new case, that information must be available. Regardless, both methods are based on producing a maximum energy or semblance display that can be directly picked to refine velocity estimates.

Figure 10-12. Angle Gather Velocity Analysis

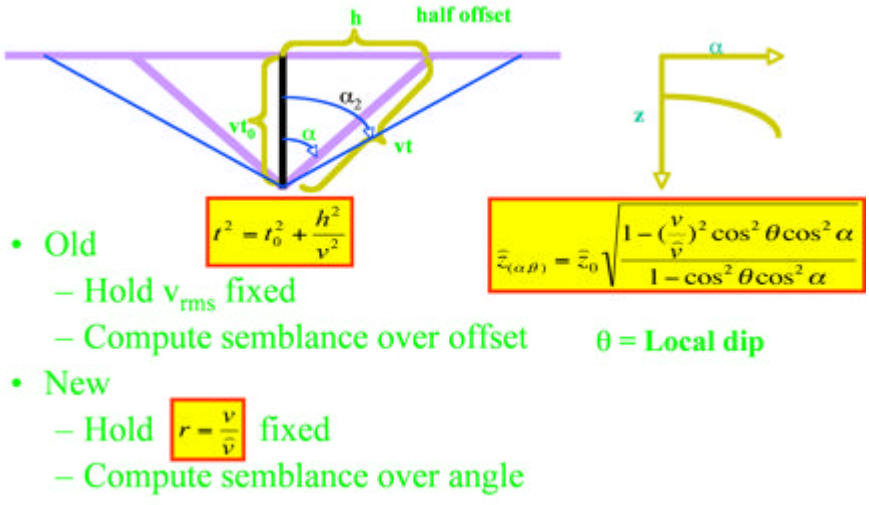

Whether we use $z(\alpha,\beta)$ or Equation 10-1, estimating v is usually based on semblance panels calculated from Equation 10-2 or Equation 10-3.

(10-1) $$t(v,h) = \sqrt{t_0^2 + \frac{h^2}{v^2}}$$

(10-2) $$s(t(v,h)) = \frac{\left(\sum_h d(x_s, x_r, t(v,h))\right)^2}{\sum_h d(x_s, x_r, t(v,h))^2}$$

(10-3) $$s(\alpha,\beta) = \frac{\left(\sum_h d(x_s, x_r, z(\alpha,\beta))\right)^2}{\sum_h d(x_s, x_r, t(\alpha,\beta))^2}$$

In this case, s is bounded between 0 and 1, but velocity at any given t or z is taken to be the value that maximize the semblance. In spite of the fact that theory underlying these equations assume flat lying reflectors, they have proven to very useful in development of seismic imaging velocity models for both time and depth imaging.

Figure 10-13(a) includes images of a depth-to-time converted SMIG, a semblance panel computed from the SMIG, the current section under analysis, and the velocity model under construction. The process of actually doing the velocity estimation is shown in Figure 10-13(b). From left to right, we see the raw depth-to-time converted SMIG and semblance panel, the picked SMIG with hyperbolic trajectories and semblance panel, and the moveout SMIG with semblance panel. This figure confirms that SMIGs can be used for migration velocity analysis and also demonstrates the current semblance based analysis process for developing short-spread velocity models.

Figure 10-13. Common image gather velocity analysis

(a). SMIG Gather, semblance panel, in progress work section, and estimated velocity model

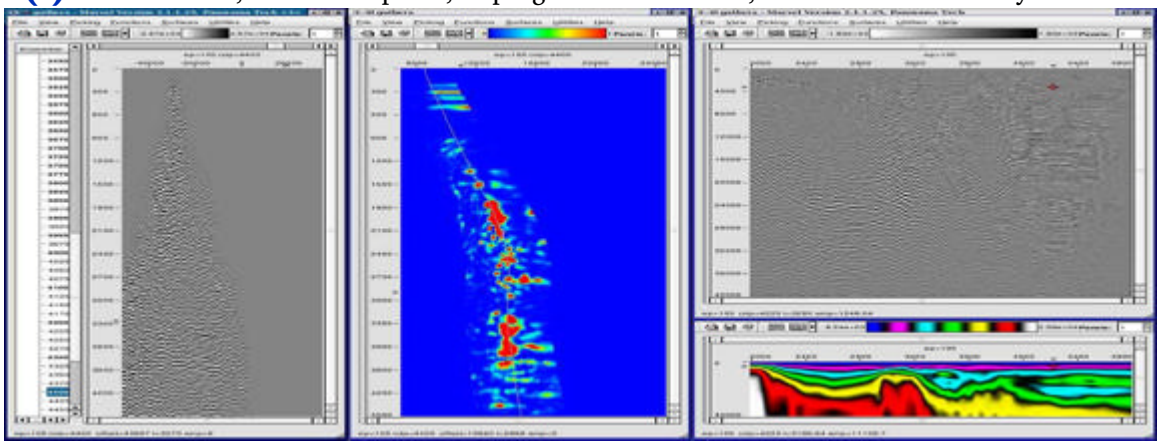

(b). Common image gather velocity analysis

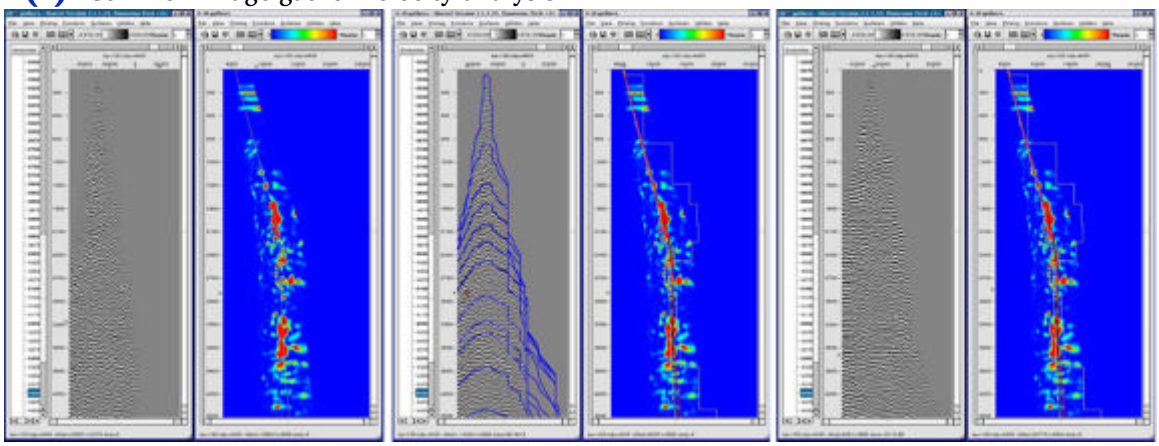

Figure 10-14 compares a common-midpoint gather, a common-midpoint gather with DMO, and a Kirchhoff depth migration common-image gather to assess the impact of partial and full migration, at least visually. The red line in the DMO stacks in (a) and (c) indicate a location where a CIG was selected for comparison. Part (a) is from an area where subsurface horizons do not dip severely, while Part (c) is from an area where subsurface horizons do dip severely. If our interpretation of the theory is correct, there should be little change in our velocity picks at (a), but considerable change for those at location (d). Changes from stacking velocity to DMO stacking velocity to migration velocity picks should be minimal in the former case and much more noticeable in the latter.

Figure 10-14. Barents Sea velocity analysis over flat and dipping horizons.

(a). Location of a CIG with relatively flat horizons

(b). Location of a CIG with steeply dipping horizons

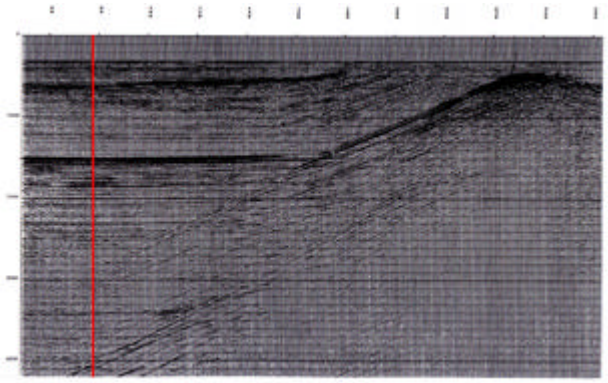

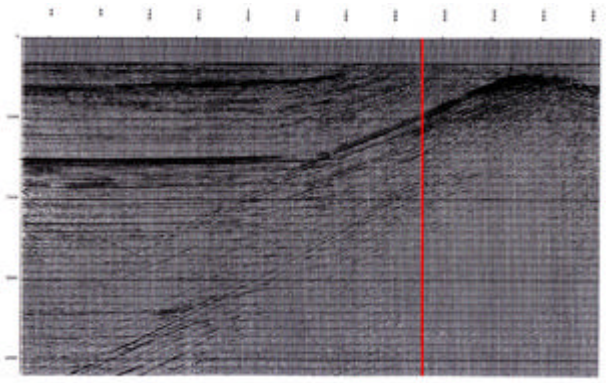

(c). Stacking, DMO, and Kirchhoff CIG semblance at (a)

(d). Stacking, DMO, and Kirchhoff CIG semblance at (b)

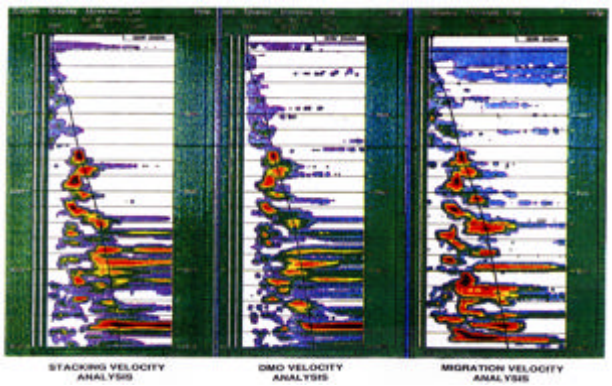

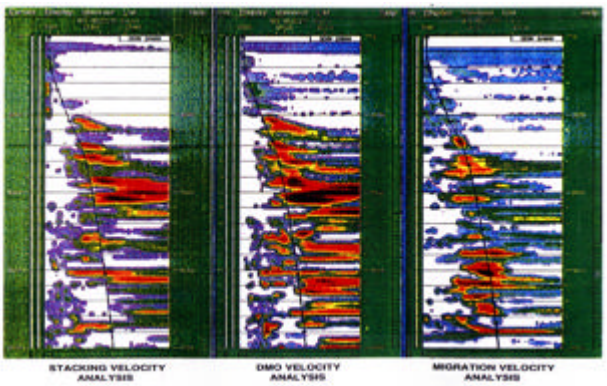

Figure 10-14(c) shows the picked curve from the migration analysis panel in (a) overlaid on the DMO panel and stacking velocity semblance panels. Note that while the panels differ in character, there is little reason to change the overall set of picks from one panel to the other. The theory seems to be reasonably solid when the horizons are flat.

In contrast to Figure 10-14(c), the picks in the panels in (d) are significantly different from each other. Even the DMO corrected panel in the middle, while better, is still

significantly different from the Kirchhoff migrated common-image gather. We would certainly be inclined to argue that stacking and DMO based velocity estimates are inferior to those obtained from this Kirchhoff based depth migration algorithm.

Figure 10-15 shows the result of three iterations of what we will ultimately call the *painless* approach to velocity model building. No horizons were used to estimate the migration velocity. While more modern migration algorithms may produce improved images, the common-image gathers are flat, and, in spite of the inability to image the base of salt, the process clearly works, even in areas where the geology is complex and the rocks are hard.

Figure 10-15. Full prestack depth migration of the Barents Sea data.

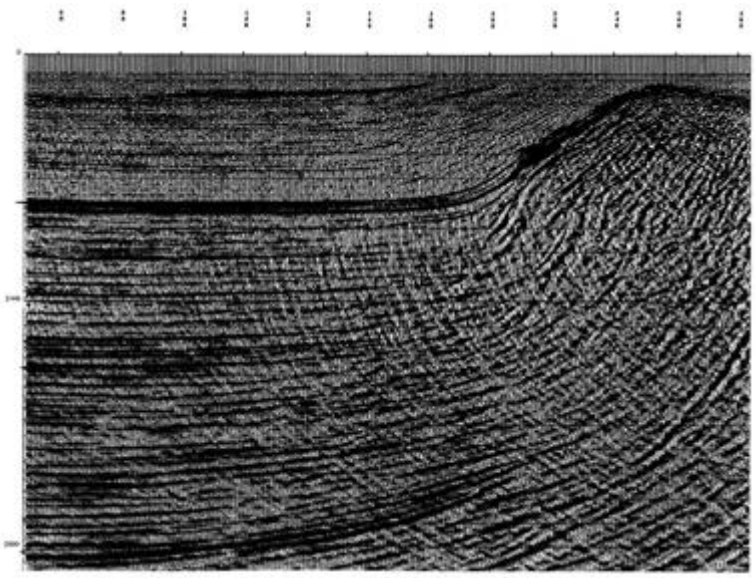

Painless (No Horizons) Velocity Model Construction

Figure 10-16 shows a typical velocity analysis-velocity model building workflow. This sequence of processes is typically used to convert data-driven-time dependent-stacking velocity estimates into depth-interval or time-RMS velocity volumes. In the painless approach, this process is carried out on flat-lying horizons, and is usually referred to as vertical updating or the Deregowski method. Since we are using a migration algorithm in an attempt to properly position events prior to velocity analysis, local dip information is usually an issue only when the lateral velocity variation is strong.

Figure 10-16. A no horizon based velocity analysis workflow

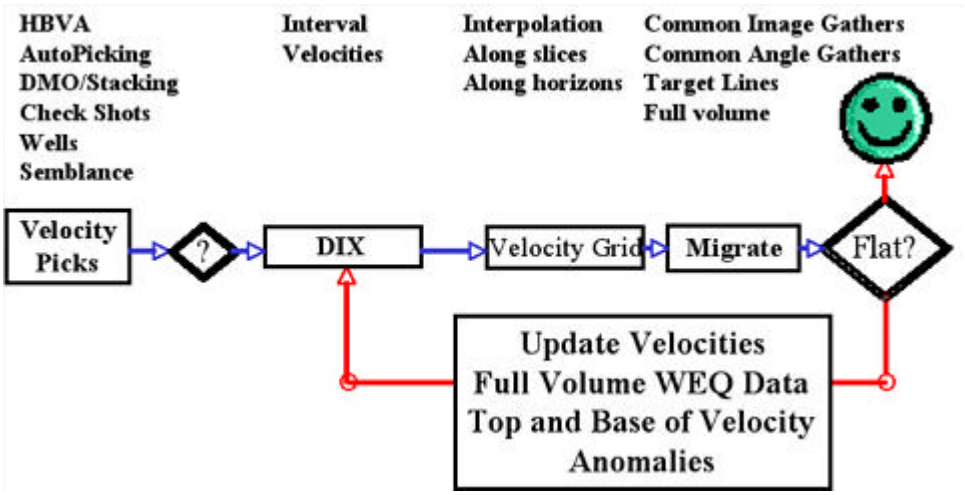

Figure 10-17 provides one approach to horizon-less velocity model construction. The idea is to directly map Dix intervals to an array of flat horizons at a user-selected fixed depth increment. Note that this Dix conversion is taking place on migrated gathers, and so should produce velocities at locations that are close to the true migrated positions. These intervals are then interpolated to a 3D model along these horizons, where a great variety of interpolation methods can be used. Such interpolation methods range from simple inverse-distance weighting to Gaussian direction oriented balls, or in some cases geostatistical prediction approaches.

Figure 10-17. Painless (no-horizon picking) approach to velocity model construction.

(a). Equally spaced flat horizons for painless picking

(b). Picked set of semblance panels

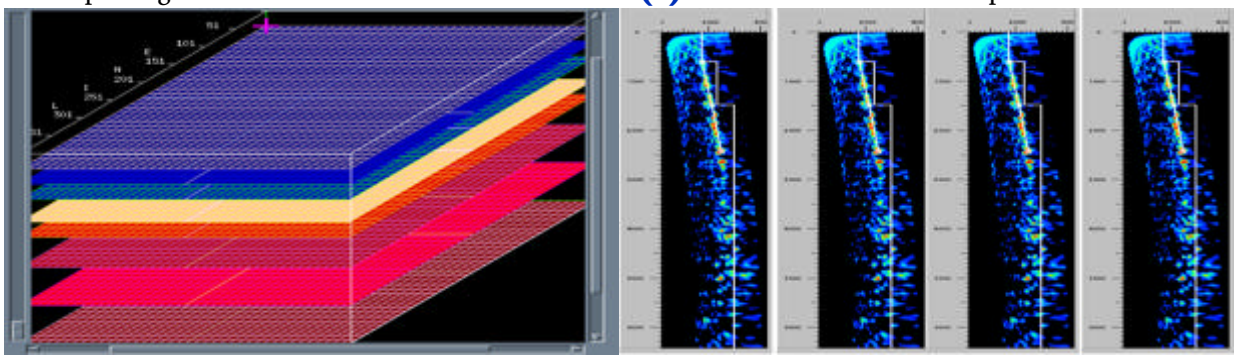

(c). Slice through the model from the initial velocity analysis

(d). Slice through the final velocity model

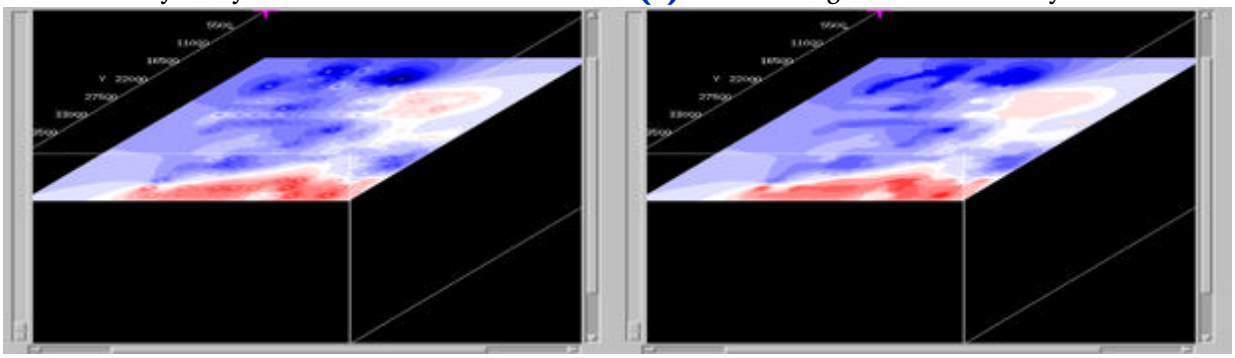

We can summarize the painless approach as follows: Begin with semblance panels like those in Figure 10-17(b). These can come from stacking velocities or velocity independent time migrations, or from depth migrations using any reasonable velocity field. When picking is complete, interpolation is used to *snap* Dix-interval velocities to each flat horizon. An example of the result of the interpolation is shown in Figure 10-17(c). The noticeable *bulls eyes* are intentional. The interpolation process was modified to ensure that these errors would produce an easy visualization of the location of the spatial velocity grid. In this case, the velocity gradient (blue to red) reflects a significant velocity change across a fault zone. No horizons were used in this process, but the velocity model still reflects local geology. Figure 10-17(d) shows a final velocity slice after three iterations. Again, the effect of geology is clearly evident in this graphic.

Figure 10-18(a) shows an initial velocity model generated using a single well hung from the water bottom. The water bottom horizon could come from a high-resolution analysis of the sea floor or from a shallow depth migration with water velocity. Typically, the well information comes from a well within the area extent of the seismic survey. In some cases, the resulting velocity field may be adjusted (sped up or slowed down) to account for depth discrepancies observed in other imaging projects.

As shown in Figure 10-18(b), MVA on CIGs can be used to painlessly update the initial well-derived velocity model. The model in (b) can then be used to perform a salt flood as shown in part (c). After the top and base of salt is determined, they can be directly inserted into the MVA updated model to obtain the final salt filled model in (d).

Figure 10-18. Well driven marine (Gulf of Mexico) velocity analysis

(a). A $v(z)$ hung off the water bottom

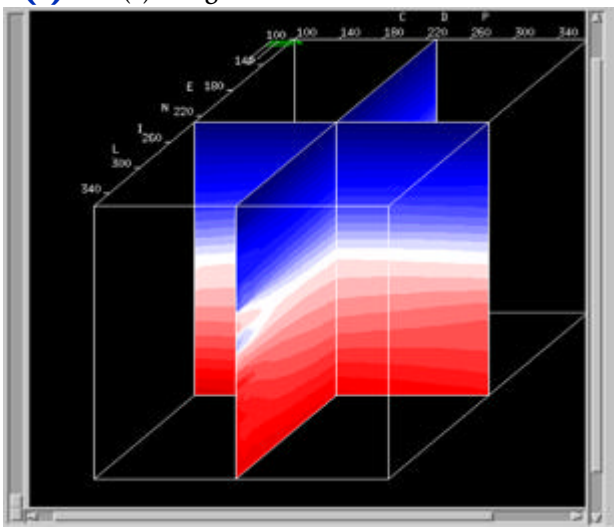

(b). Painless velocity update

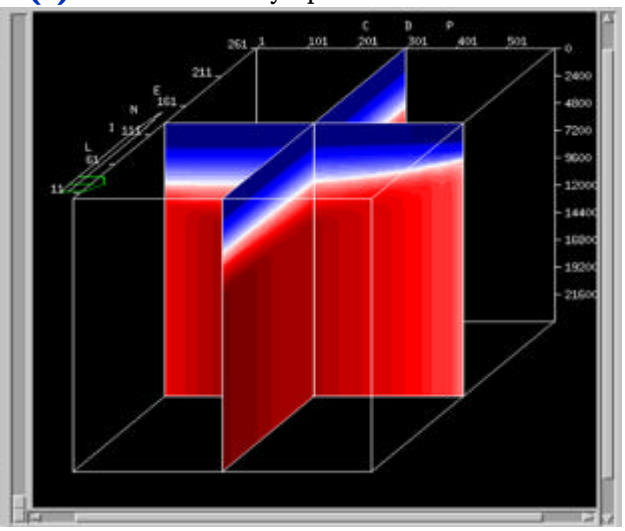

(c). A “salt flood” migration

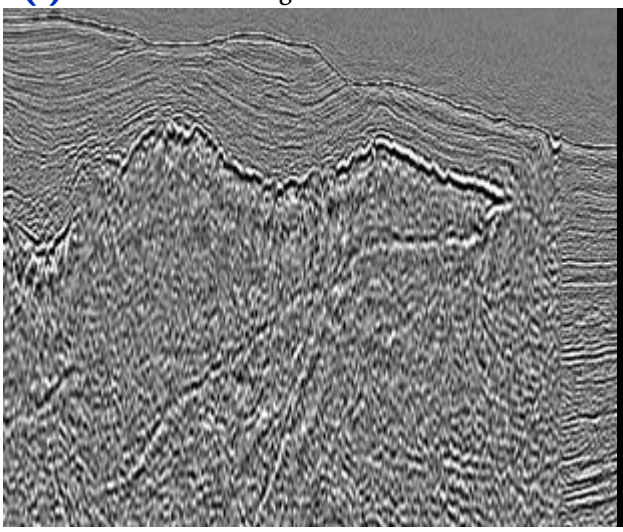

(d). Salt body insert

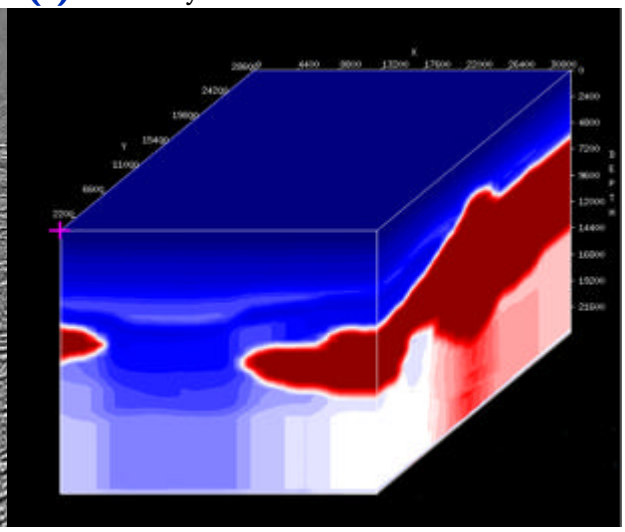

Figure 10-19(a) is a final image based on the process described in Figure 10-18. This volume was the result of a common azimuth migration. Note the excellent definition of the top, the base, and the subsalt reflectors. The associated flat image gathers in Figure 10-19(b) show that the painless approach to Earth model estimation can be quite successful.

Figure 10-19. Full volume common azimuth migration and associated image gathers.

(a). Full volume common azimuth migration

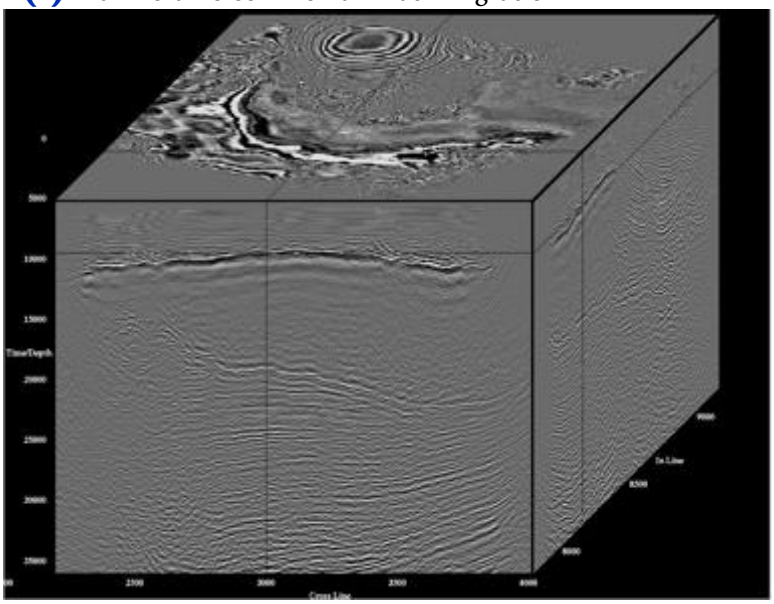

(b). Common image gathers from the migration in (a)

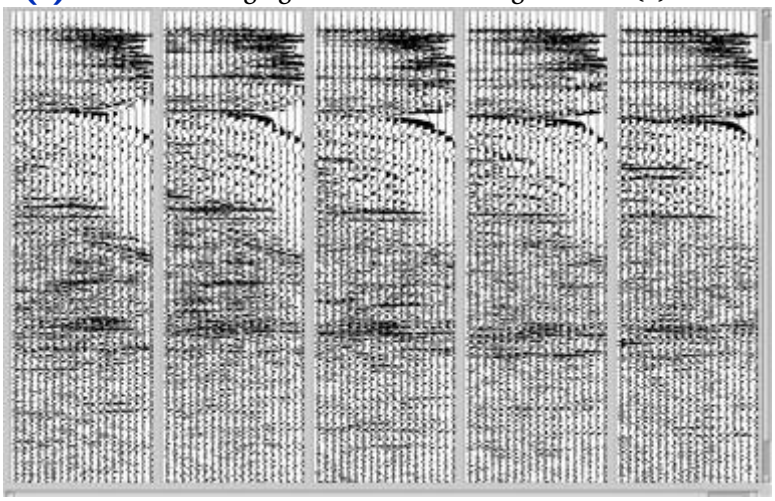

As detailed in Figure 10-20 (b), prestack time imaging can frequently be done using the painless approach with automatically picked CIGs. When the input data is of high quality, automatic picking can be a useful tool to both assess the need for preprocessing and to quickly provide a useable image.

Figure 10-20. Automatically picked prestack Kirchhoff time migration.

(a). Autopicked CIGs **(b).** Prestack time migration via autopicking

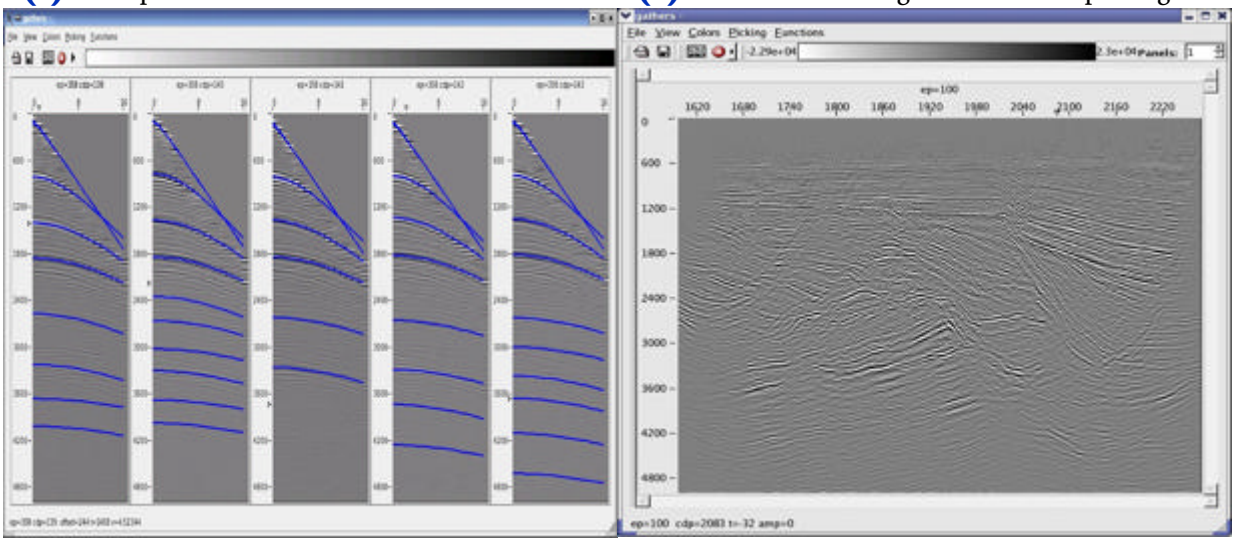

Horizon-Based Velocity Analysis

So the question is: *Do we ever need horizons?*

In some sense, the answer is driven by how well we can flatten the gathers we output from the Deregowski loop. It is great when the painless method does a good job of flattening the gathers because horizons certainly create a plethora of problems in an iterative scheme for velocity estimation. We would like to avoid these problems in all situations. Horizons change shape and position every time a new Earth model is part of a re-migration of the original input data. The processor is then either forced to reinterpret a new set of horizons or to edit the existing set prior to another iteration of velocity analysis. It would certainly be nice never to have to worry about horizons. There are also geologic environments where horizons are just as useless as the painless approach in those environments, but it is also probably true that in this kind of regime, nothing will produce acceptable results.

There are certainly many geologic settings where the use of horizons is absolutely necessary. Horizons are essential when strong, visible velocity anomalies, such as salt domes and sills, are present. The tops, sides, and bottoms of these visible bodies are

interpreted, defined as horizons and inserted into an existing Earth model. Figure 10-21 shows how the top of salt is interpreted in a salt flood exercise.

Figure 10-21. Horizon interpretation for a salt flood.

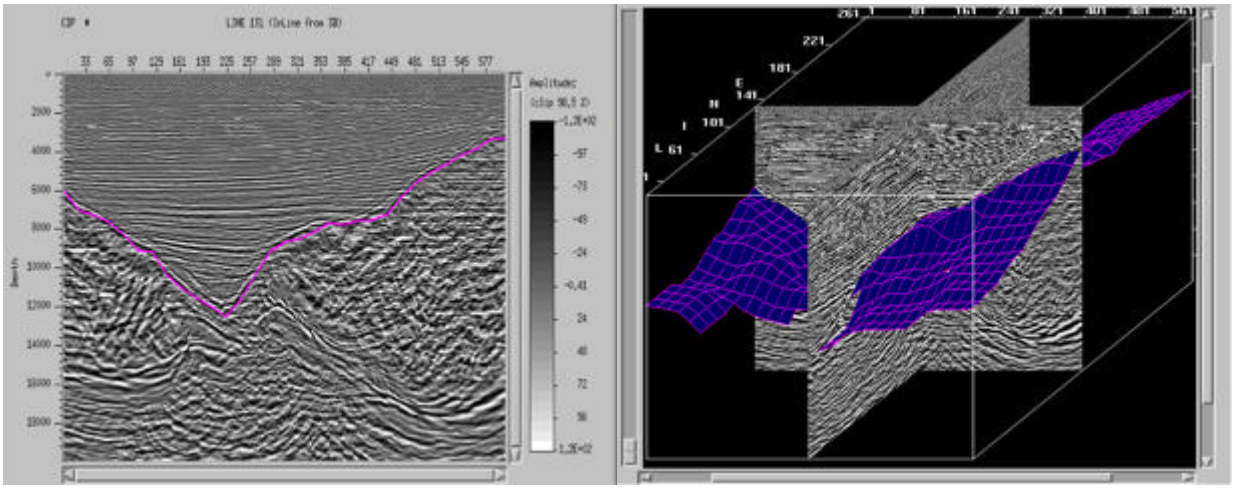

Horizons are probably also essential when velocity anomalies are invisible. In this case, we cannot interpret the tops, sides and bottoms, so horizons above and below the suspected area are the only option. In certain geologic settings, most notably in areas with strong carbonate bedding, fast velocities within relatively thin sections require utilization of interpreted horizons to produce adequate estimates of the velocity within the bedding planes. When data-based estimates are insufficient, horizons may also be useful as control surfaces allowing constant velocity insertion between specific layers to define a more accurate Earth model. Perhaps the most important setting where horizons are required is when it becomes clear that the painless approach has failed miserably. In this case, it is probable that an attempt to apply tomographic inversion will also be recommended. However, there are always exceptions to almost every rule. In geologic environments where subtle velocity variations are not easily seen, we may have to resort to more extreme approaches. This would definitely include very fine horizon based velocity model construction along with full utilization of tomography.

Figure 10-21 is an illustration of the interpretation of horizons on top of a base of salt. This kind of interpretation is also necessary for certain kinds of residual tomography. Typically, a reasonable set of horizons provides tomographic inversion with precisely the information necessary for success. It is not necessary to be as accurate as we might be for prospect generation, but it is necessary to define as many horizons as possible.

Once horizons have been defined, velocity picking can be done along the horizons themselves. While this should produce horizon consistent velocities, vertical updating through the Dix equation is still necessary to provide the required interval velocity estimates above the horizon under analysis.

Figure 10-22 shows the kind of model produced from a typical horizon based approach. It is difficult to believe that the blocky nature of this model is realistic. Because they use high frequency approximations, raytracers have considerable difficulty calculating accurate traveltimes unless the model is smoothed. The only real way to avoid the blocky nature evident in this image is to interpret a large number of densely spaced horizons or to insert a large number of invisible horizons between relatively sparse sets. Interpreting a large number of horizons requires a considerable amount of human time and cost. Interpolation of a fine set of horizons between sparse data seems to be moving back toward a more painless methodology. However, in situations where compaction plays an important role in vertical velocity variation, forcing the velocity structure to follow horizons when they are not the chief defining factor can be disastrous.

Figure 10-22. A horizon based velocity model

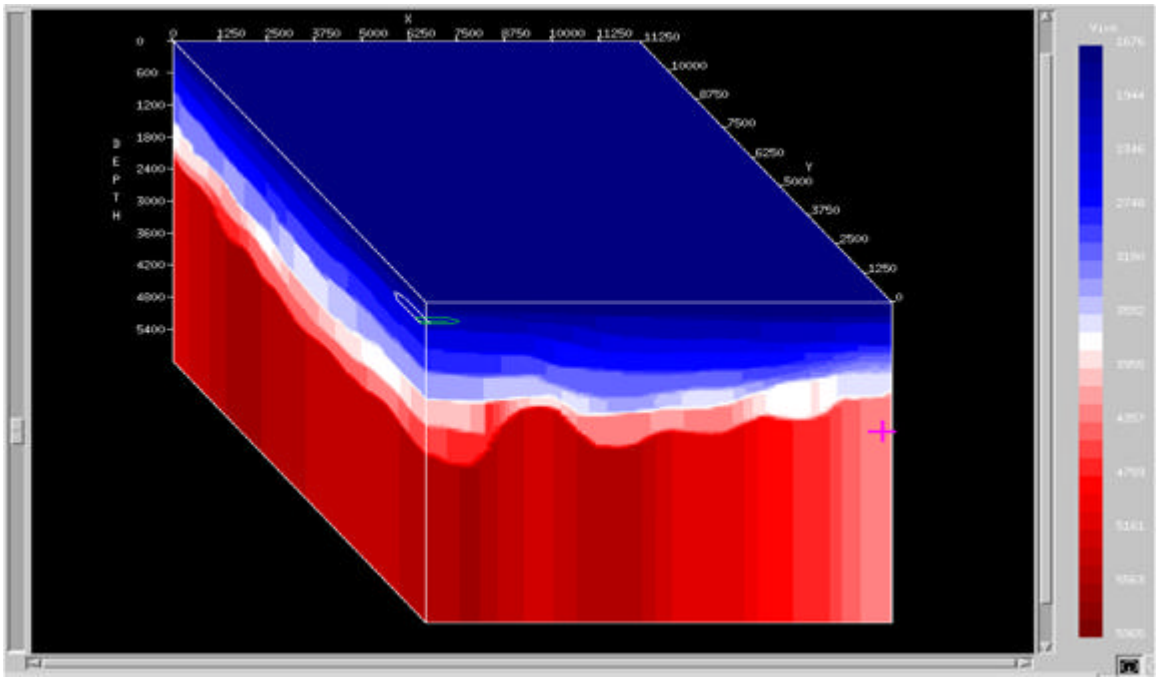

In Figure 10-23, we see a set of gathers that have been through several iterations of vertical or Dix updating. Note that the gathers on the right are reasonably flat while those on the left are not flat. Because these gathers produce poor images when stacked, this phenomenon cannot be improved by traditional horizon-based vertical methods. This three-dimensional effect was ultimately resolved only by careful application of tomography. While there are many approaches to tomography, recent experience has shown that residual methods work best. Residual approaches are usually applied only after an initial migration velocity volume is available. They also normally require reasonable information about local dip, which can be obtained from a horizon-based approach, or by direct estimation of the local dip from the current image, or from specific geologic knowledge. Since horizon-based methods tend to offer better accuracy than direct automatic estimation, we restrict our attention to that methodology. Note that this implicitly assumes some form of geologic interpretation of the study area.

Figure 10-23. Non flat gathers.

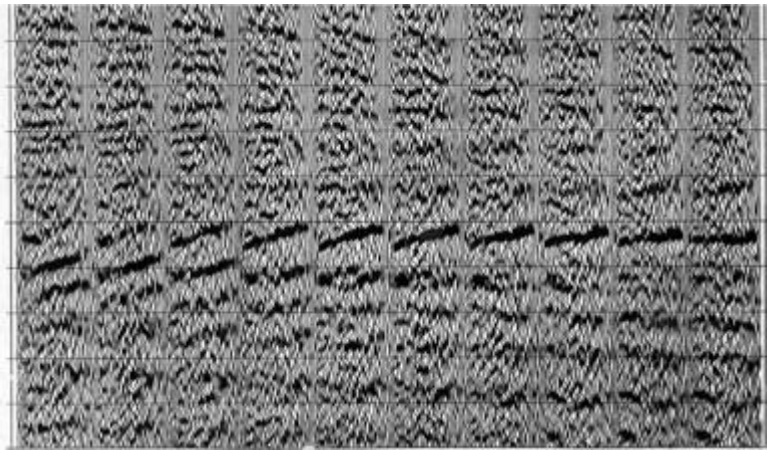

Figure 10-24 shows a typical horizon-based velocity analysis–velocity model building workflow. This sequence of processes is almost identical to that in Figure 10-16 on page 270, except that velocities are “snapped” to user-defined horizons rather than to an equally spaced set of flat horizons. Perhaps one benefit to this kind of analysis is that once the process has reached a stationary point, all the necessary information required to apply tomography is in place.

Figure 10-24. A horizon based velocity analysis workflow

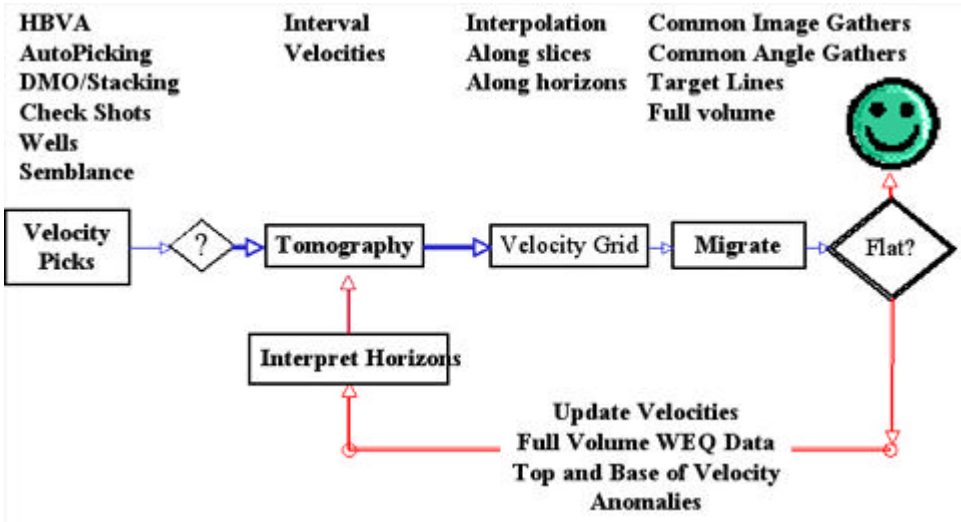

Residual Tomography

The basic geometry of residual-seismic tomography is explained by Figure 10-25. We see two source-image-point-receiver raypaths, one in red at a short offset and one in green at a longer offset,. These raypaths represent the migrated location of a reflector at each of these offsets. As each of these rays pass through the cells of the gridded model, it is possible to calculated the total distance traveled from source to receiver for the current migration velocity model.

Figure 10-25. Tomographic Geometry

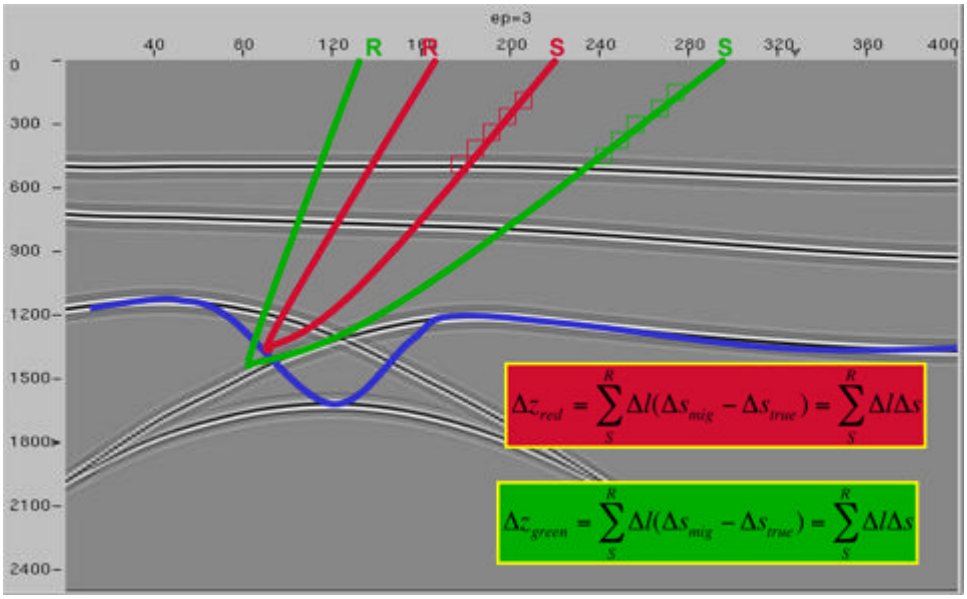

Whether calculated for the red or the green ray, that distance, d, is given by Equation 10-4, where Δl is the length of the ray in any given grid cell and Δs_{mig} is the actual migration velocity in that cell.

(10-4)
$$d = \sum_{S}^{R} \Delta l \Delta s_{mig}$$

What we are interested in finding is the true velocity, Δs_{true}. To do this, we calculate Δz for each ray path in the model using Equation 10-5.

(10-5)
$$\Delta z = \sum_{S}^{R} \Delta l(\Delta s_{mig} - \Delta s_{true})$$

Note that we can measure Δz for each horizon on a CIG, and so we assume we know this value for each and every possible ray. Algebraically, Equation 10-5 is a matrix equation

of the form shown in Equation 10-6, and it can be solved for Δs.

(10-6) $$\mathbf{A}\Delta\mathbf{s} = \mathbf{Z}$$

Once Δs is known, computation of s_{true} is straightforward.

In many respects, seismic tomography is very similar to common computer aided tomography (CAT) scans. The primary difference between the two is that CAT scans record purely transmitted energy, while seismic tomography is reflection based. Computer aided tomography reconstructs an image of human tissue by back projecting recorded transmission energy over a straight line. Seismic tomography back projects over a reflection cone. Seismic tomography is also a residual technique. It does not use directly recorded information to estimate the Earth model, and is always based on information extracted from an existing imaging exercise.

Figure 10-26(a) is an example of residual tomography as it would apply to residual offset dependent depth differences at two line and crossline locations. The figure shows back projected ray bundles indicating changes in velocity as a function of offset from the central line and crossline location.

Figure 10-26. Fundamentals of residual tomography

(a). Tomographic back projection

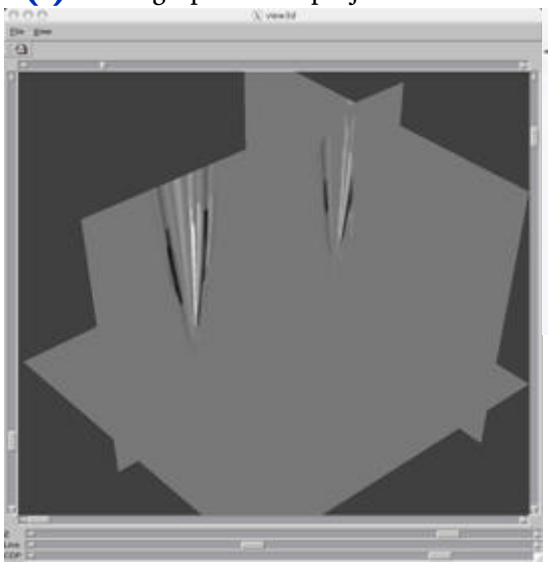

(b). Tomographic geometry

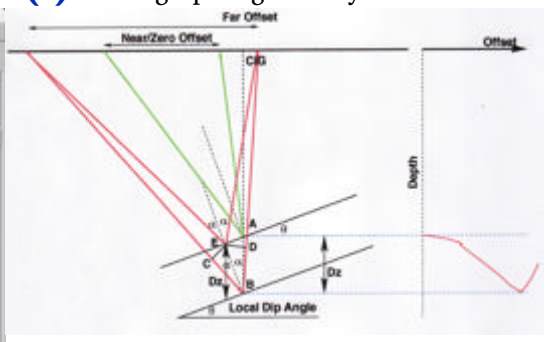

Residual tomography, as shown in Figure 10-26(b), is based on the assumption that after a prestack depth migration with velocities that are close to each other, lateral positioning of subsurface events will also be close to correct. This being the case, we can relate differences in depth differences as a function of offset to a residual velocity or slowness increment needed to make the arrival on the common image gather flat. To do so, we need to have reasonable estimates of the local dip everywhere in the volume

being analyzed. In this figure, the correct or reference dip is measured correctly at the offset determined by the near zero-offset trace (the green rays). What we measure is the residual depth difference at some other offset (the red rays). If we know the local dip, all this information can be related to a change in velocity that forces the next migration to produce much flatter common-image gathers.

Thus, the input required to perform a residual tomographic inversion is:

- a reasonable migration velocity field
- a picked set of residual depths
- a good set of horizons or some other method for estimating local dip. If horizons are used, there should be as many horizons as possible.

Figure 10-27 shows what we need to measure to have the proper information to use the method outlined in the previous figures. The right hand side of this figure is a common-image gather after a migration with an incorrect velocity. Note that the curved arrival is close to parabolic or even hyperbolic in shape, but is definitely not flat. The curved green line marks residual depth differences in reference to the shortest arrival. Because the arrival curves down, we know that a velocity above the horizon is too slow to properly correct the horizon at all offsets. Had it curved upward, the velocity in question would have been too fast. Knowing that the velocity is too slow is one thing, but knowing where it is too slow is another thing entirely. What residual tomography does is use redundancy of estimation to determine where to change the velocity to produce flat arrivals. This means that to be effective, tomographic inversion must have sufficient redundancy to do its job. This, in turn, means that we must solve a huge tomographic problem. It also means that a good tomographic solver will have been designed to work from automatically-picked residuals.

Figure 10-27. Residual depths as input to tomography.

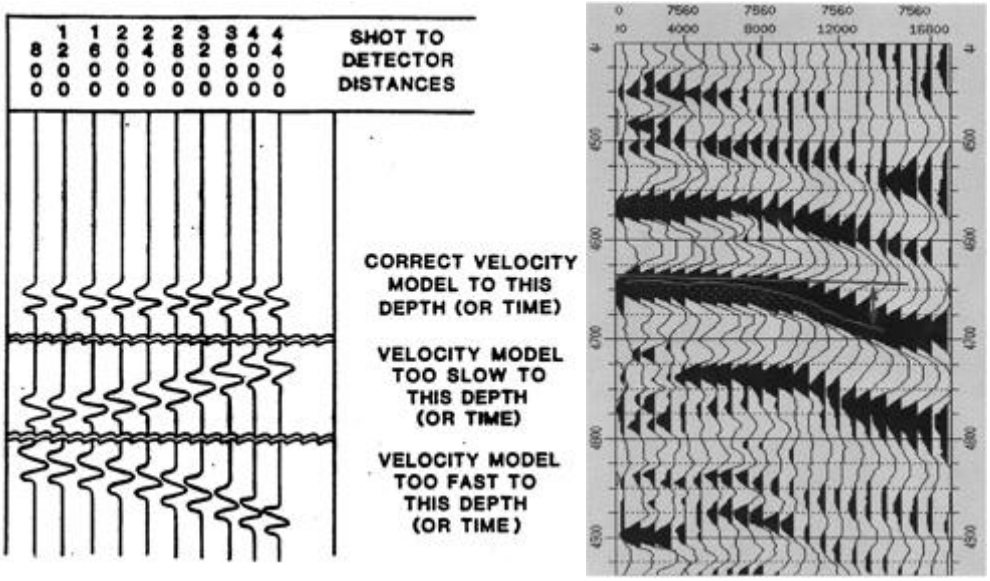

Figure 10-28 is an example of the use of automatic dip estimation and flattening on a set of CDPs from the SEG AA′ data set. Parts (a) and (b) of this figure are illustrative CDPs and their flattened counterparts. Figure 10-28(c) is the result of stacking the entire suite of CDPs in the line.

Figure 10-28. Automatic dip estimation, flattening and stacking.

(a). SEG AA′ Gathers before dip

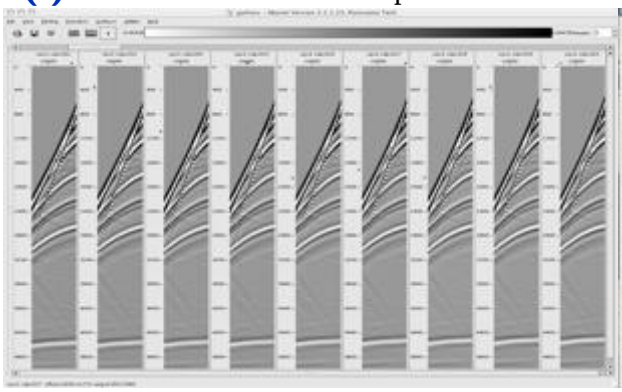

(b). SEG AA′ Gathers after dip

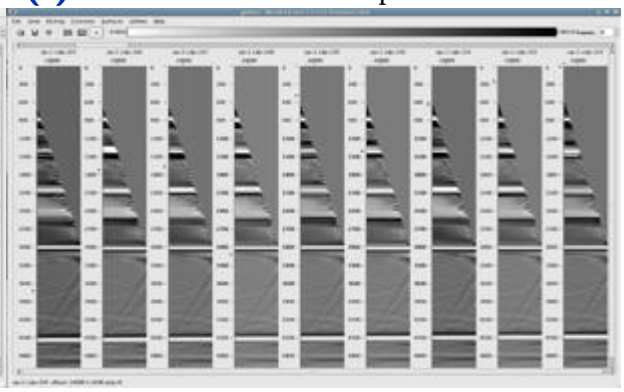

(c). SEG AA′ Auto Stack after dip

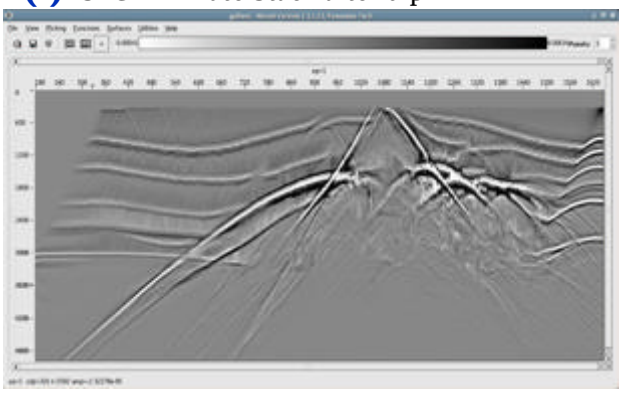

Figure 10-29 is for illustrative purposes only. Residual depths are estimated along horizons. Clearly there is no need for residual tomography at these locations. The colored lines just indicate the depths at which horizons intersect each offset plane.

Figure 10-29. Residual moveout along a horizon. This is Horizon Based Velocity Analysis or HBVA.

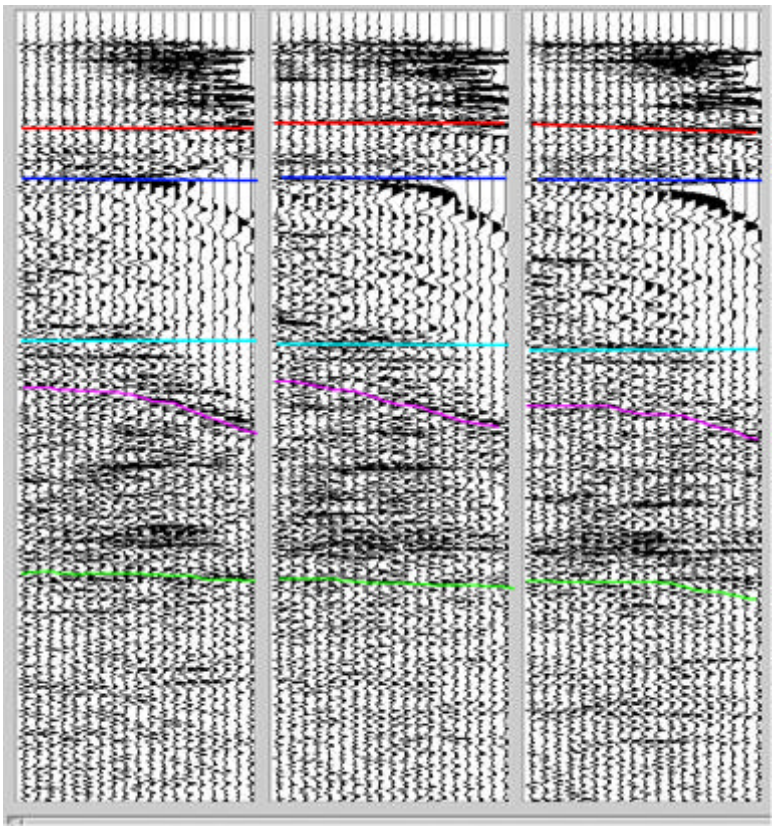

In certain cases, migrating along a predefined horizon (slab migration) reduces computation time and results in faster turnaround time. Figure 10-30 shows the stack of data migrated along a given 3D surface.

Figure 10-30. Imaging Along a Slab

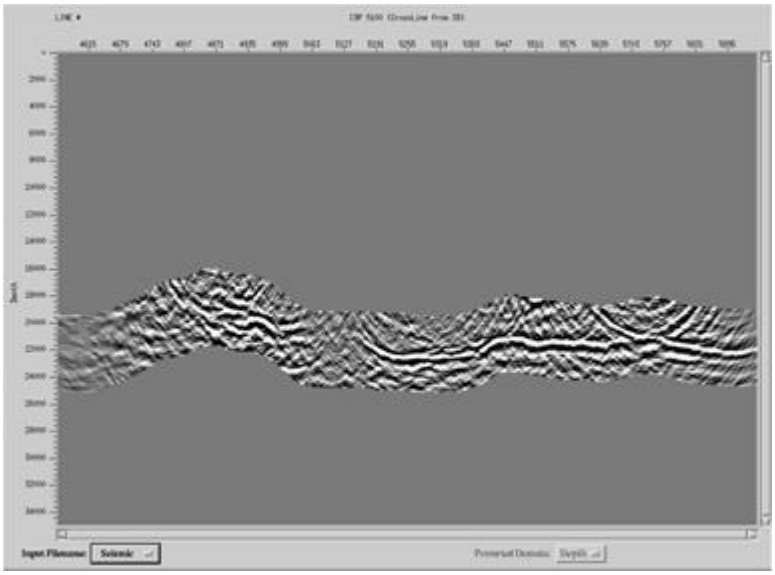

Performing percentage-based migration over a horizon can result in horizon-based analysis similar to that shown in Figure 10-31.

Figure 10-31. Residual Moveout Along Horizons

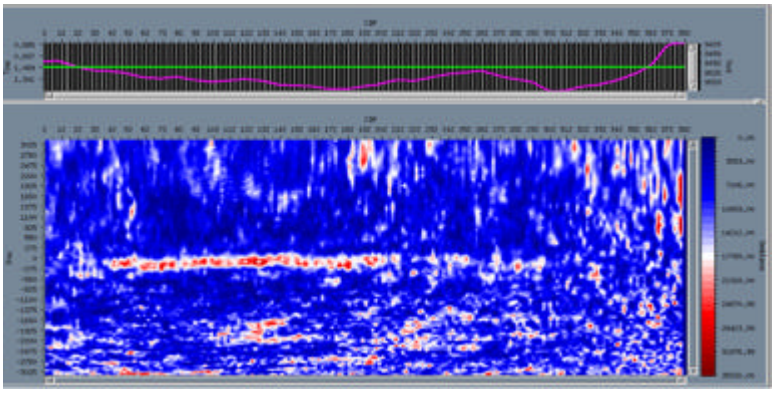

Tomographic updating should not be considered to be a technology that solves all velocity update problems. Like its semblance-based counterpart, tomographic accuracy is dependent on the angle range at any given point reflector. As depth increases, this angle range decreases in width until it is too narrow to be of value. Once the angle range reaches a width of less than 10 degrees, tomography is no more useful than traditional semblance-based analysis.

Tomography works best when at any given depth slice, its back projected cones, as displayed in Figure 10-26 on page 279, overlap. Again, as depth increases, the degree of overlap decrease and thereby reduces the effectiveness of the tomographic update. Some of these issues can be handled through interpolation or physical and geologic constraints of the type illustrated in Figure 10-32, but little can be done about the angle range.

Figure 10-32. Natural Tomographic Constraints

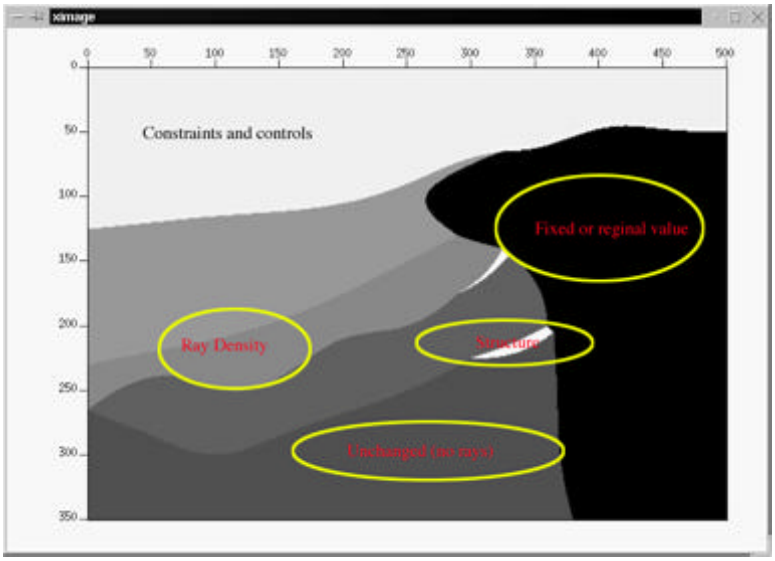

Figure 10-33 shows the tomographic exercise in graphical form. The left side of Figure 10-33 shows the horizons which were picked from the initial Dix-based velocity updating. The center graphic of this figure shows the residual depth differences from an automatic picker. The rightmost image in the figure] shows the updated velocity model after the completion of a residual tomographic update. Compare this to the original velocity field in a past slide.

Figure 10-33. Horizon Based Tomography

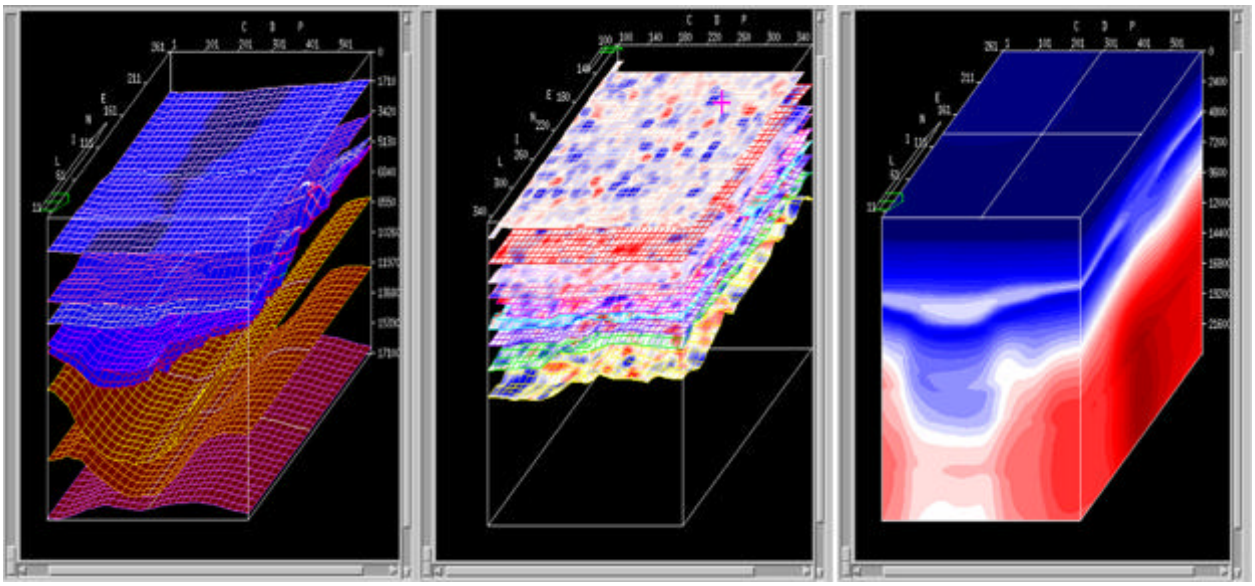

Figure 10-34 contains a side-by-side comparison between a vertical and a tomographic update. The vertical update is on the left and the tomographic update is on the right. Note the velocity inversion (the green on the right hand side of the right figure) and the increased dips roughly in the middle of the right-most figure. This data is over a granitic overthrust in the state of Wyoming in the USA.

Figure 10-34. Vertical versus Tomographic Velocity Update

(a). Vertical Update **(b).** Tomographic Update

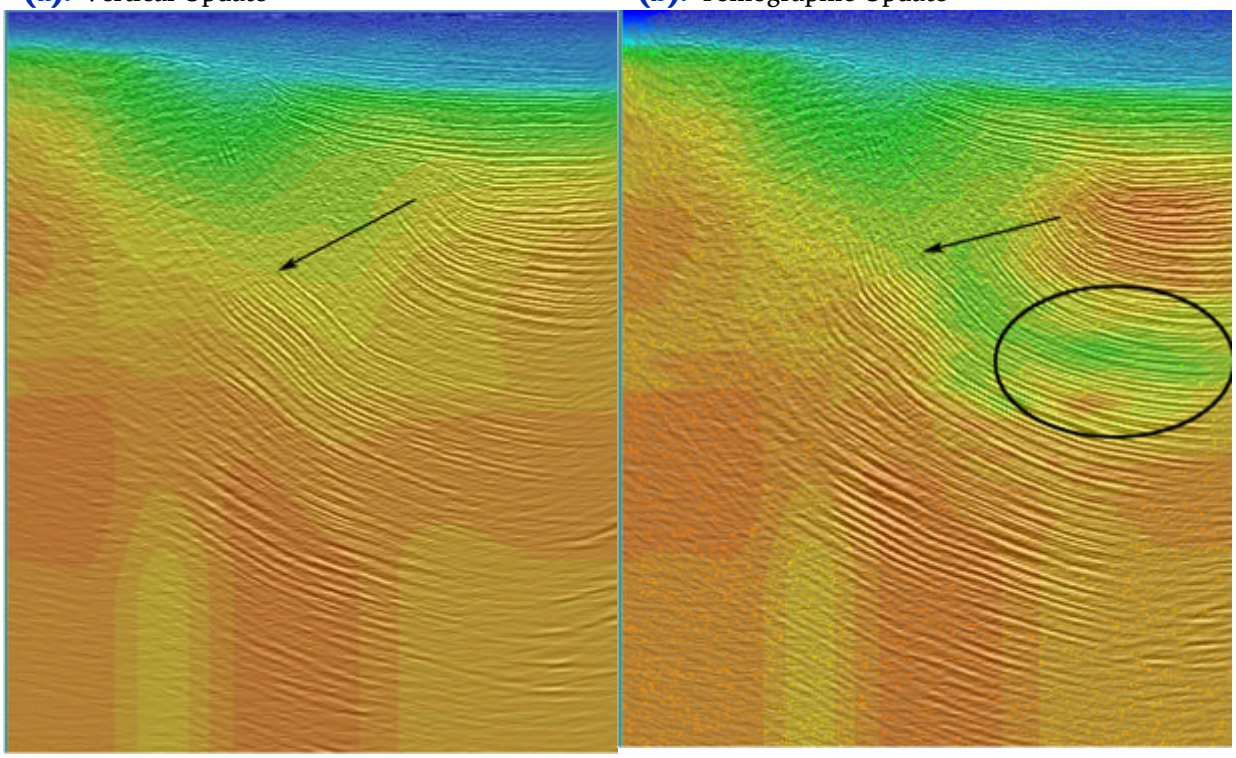

Figure 10-35 is an idealized flowchart summarizing the concepts and ideas discussed in this part of the course. The first part of this slide embodies what might be called vertical updating. It is only at the bottom the figure that we actually begin the option to use tomographic updating. Note that tomography is applied only when there is sufficient residual curvature in the output gathers to warrant it. Velocity defined structures, such as salt, are updated through velocity floods. After the top and base of the anomaly is well defined, residual tomography can be re-applied as needed.

Figure 10-35. Painless Model Estimation Finalized Workflow

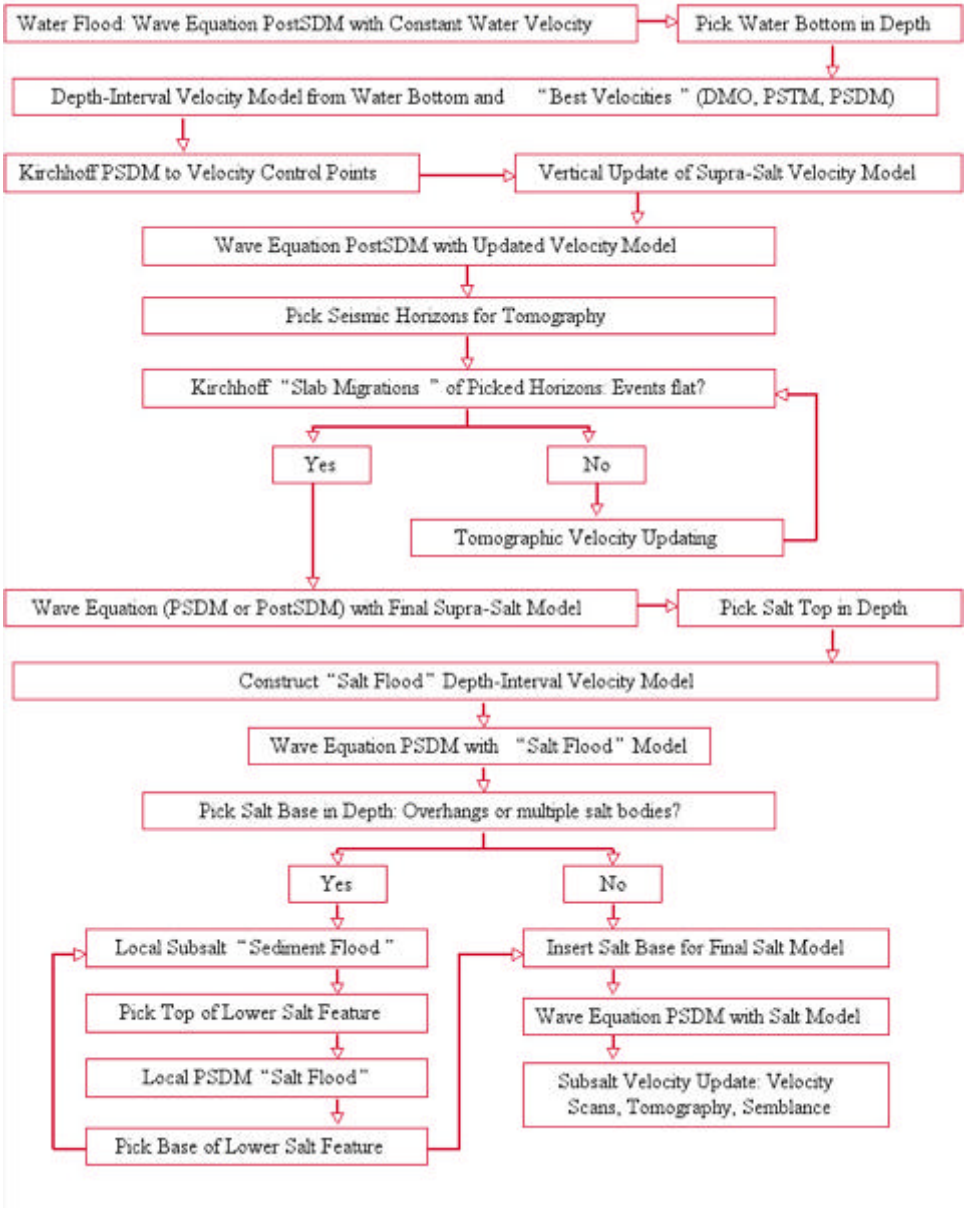

An essential feature of velocity model construction in hard rocks or on land is the increased utilization of wells when available. What is important for this book is the fact that depth migration continues to play its part in the ultimate velocity model definition. In some sense, Figure 10-36 is more or less identical to the previous soft-model slide. The only real difference is when wells are present is to convert the well information so that it matches seismic times. We can think of this process as check-shot correction, but it is just as easy to do when events at specific times can be matched to specific depths on borehole data. Frequently, velocity anomalies can be resolved in much the same manner as those caused by salt structures in the Gulf of Mexico.

Figure 10-36. Hard Rock Horizon Based Model Estimation Finalized Workflow

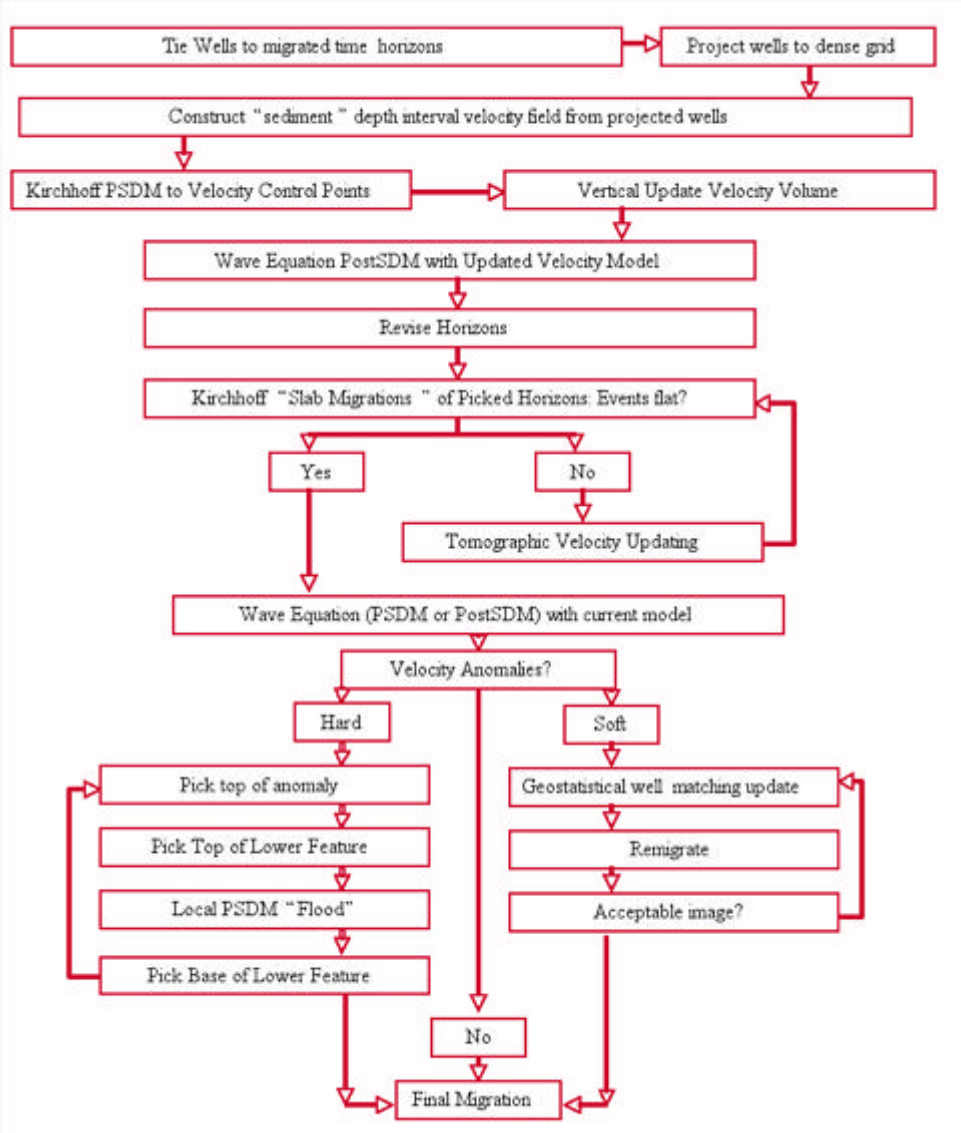

SEG AA′ Case Study

At this point, previous work flows and schemes for estimating depth migration velocity fields may seem a bit daunting. It is probably worth going through the process on a couple of selected synthetic examples where we know what the answer is. Our first example is based on the so-called SEG AA′ synthetic. It is really not proper to begin by showing the true velocity model at the start of this exercise, but the interested reader can find that image near the end of this section. An automatically stacked version of the input data is shown in Figure 10-28.

Figure 10-37. SEG AA′ coarsely picked background velocity (every 200).

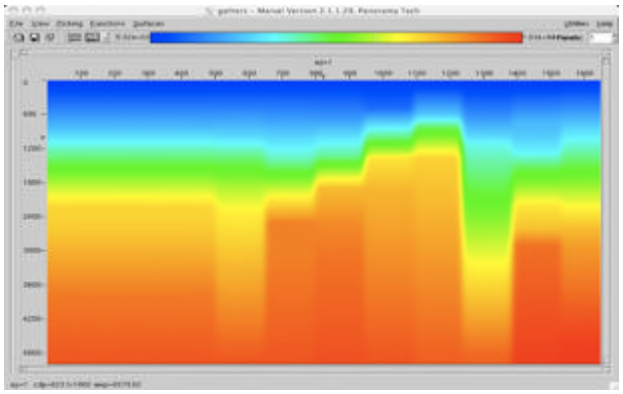

Figure 10-38. SEG AA′ First Iteration Auto Picking

(a). SEG AA′ Auto Picked CDP

(b). SEG AA′ Auto Picked Semblence

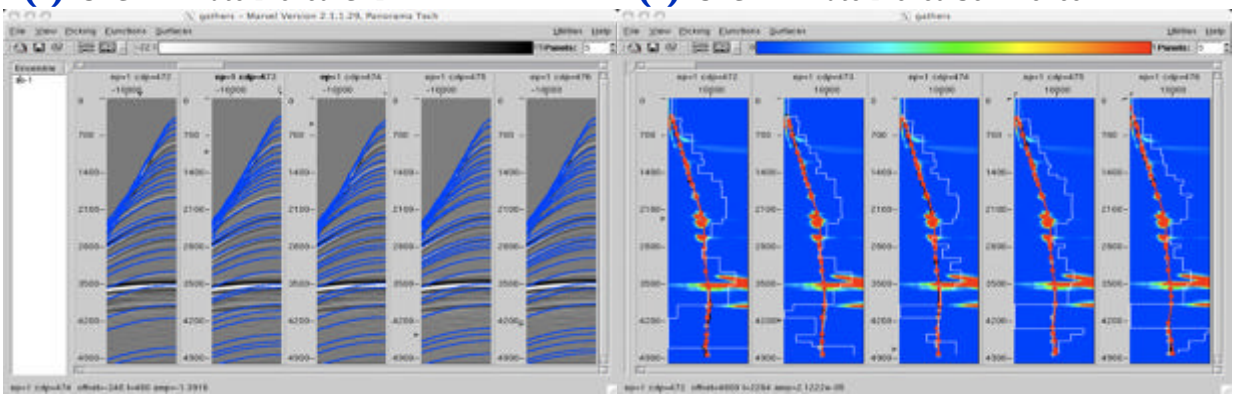

Figure 10-39. SEG AA′ First Iteration Auto Picked Models and Kirchhoff PSDM.

(a). SEG AA′ Auto Picked RMS **(b).** SEG AA′ Auto Picked Depth **(c).** SEG AA′ Migration using (b)

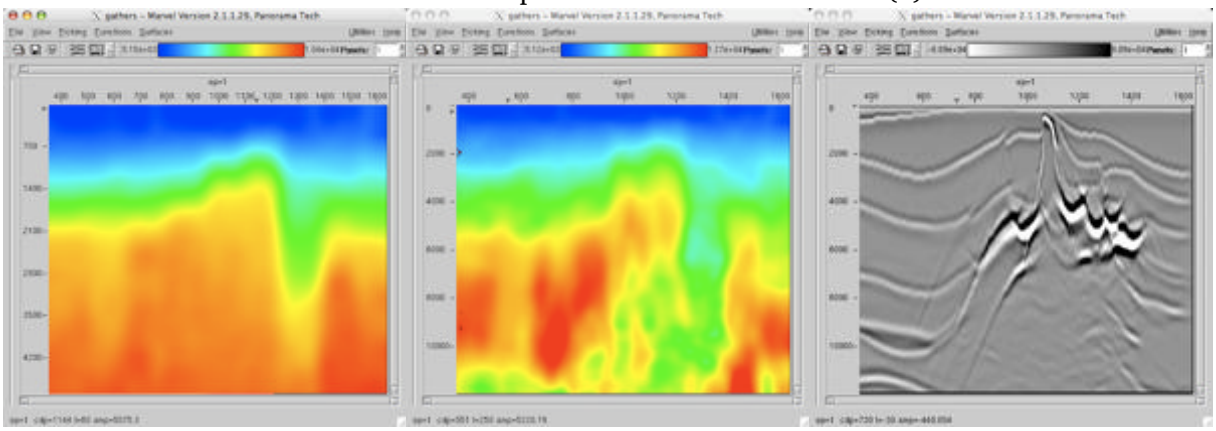

We start the process by first estimating a pre-stack time velocity profile, converting that to depth and then performing a migration of the recorded data. Figure 10-37 shows a stacking velocity model constructed by picking every 200th CDP from the input data. This is clearly a very coarse model, but its real purpose is to give us a background for automatic picking of the SEG AA′ input data. Figure 10-38(a) shows a selection of automatically picked gathers, while the graphic in (b) illustrates the corresponding semblance panels. The automatic picking used the model in Figure 10-37 to tightly constrain the picks. Thus, it is not surprising that the stacking velocity model in Figure 10-39(a) does not vary much from the coarse hand-picked model in Figure 10-37. The interval velocity model in Figure 10-39(b) was used to migrate and obtain the image in part (c).

It is clear that we need to repeat this picking process in hopes of improving our image substantially. To this end, we first use the model in Figure 10-39(b) to time-to-depth convert and apply inverse NMO. Figure 10-40 illustrates the process. The set of common image gathers (CIGs) in part (a) of this figure show that the initial stacking velocity analysis did not produce a very good model. The gathers are not flat and, in fact, appear to have little or no NMO correction. However, the fully inverse NMO corrected gathers in Figure 10-40(b) have considerably more moveout, so the migration did improve the flatness of the gathers to some extent. Parts (c) and (d) of Figure 10-40 are the automatically picked gathers and semblance functions from the inverse NMO corrected time-gathers.

Figure 10-40. SEG AA′ Autopicked First Iteration CIGs and Semblance

(a). 1st Auto Picked PSDM CIG

(b). 1st Auto Picked PSDM CIG after INMO

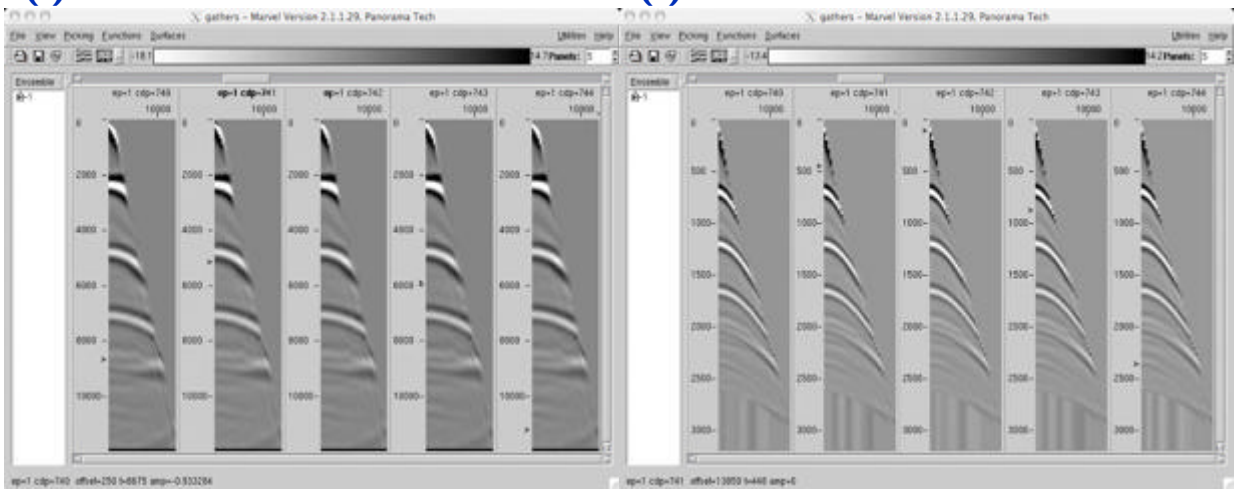

(c). 1st Auto Picked PSDM CIG

(d). 1st Auto Picked PSDM CIG Semblence

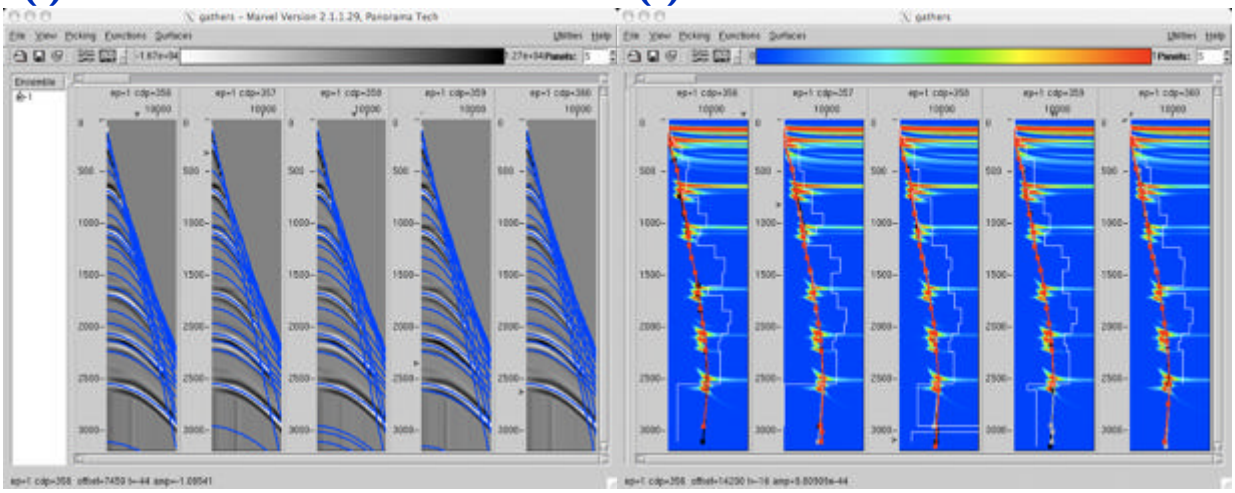

The newly computed velocity model from these picks is displayed in Figure 10-41(a) and the newly computed image based on this model is shown in part (b). A careful review of the CIGs from this second iteration suggested that it was time to estimate and insert the salt top and base. To this end, the top of salt was picked from the image in Figure 10-41(b). The salt flood based on the top of salt surface is displayed in Figure 10-41(c) and the resulting salt flood image is in part (c). The base of salt was defined from the image in Figure 10-41(c) and the resulting salt body inserted into the model in (a). The result is shown in Figure 10-41(d). Part (e) is the image based on the model in (d).

Figure 10-41. SEG AA′ Second Iteration Autopicked Models and Section

(a). 2nd Auto Picked Model

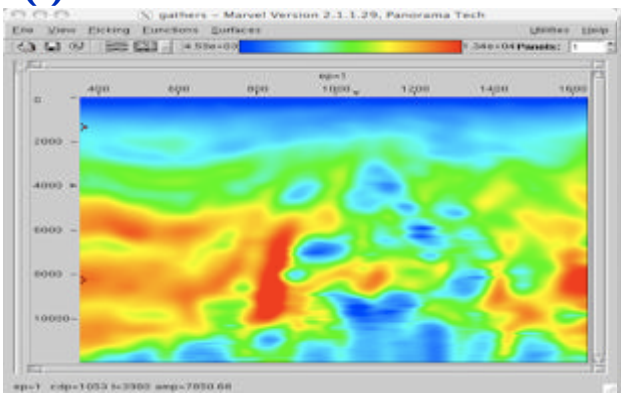

(b). 2nd Auto Picked Model Image

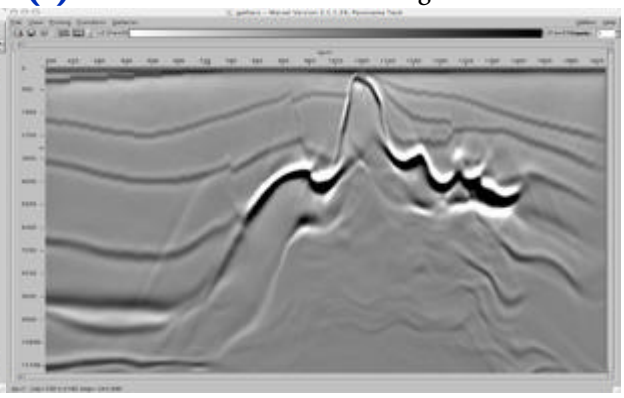

(c). 2nd Auto Picked Salt Flood Model

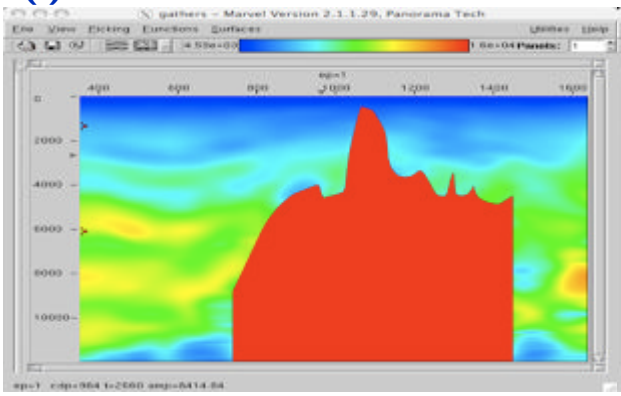

(d). 2nd Auto Picked Salt Flood Image

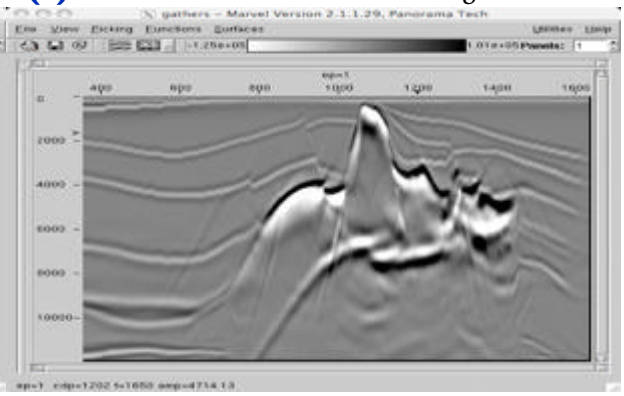

(e). 2nd Auto Picked Depth

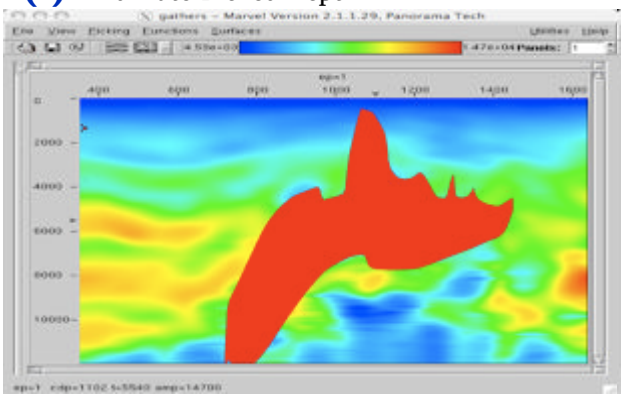

(f). 2nd Auto Picked Depth

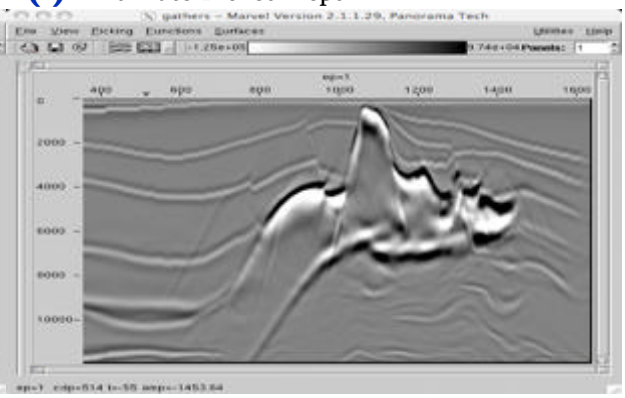

At this point, it is clear that the crude picking, Dix inversion-migration process has produced a reasonable image of what we might call sediments and the salt structure. It is also clear that the image below the salt is not fully sensible geologically. We would think that the way forward would be to keep the salt body in place and complete a very careful re-picking of the CIGs below salt. Unfortunately, the offset range was somewhat limited and almost any velocity below salt produces some kind of image.

Thus, it appears that our only option is to perform several additional migrations using models constructed with percentage differences or maybe even constant velocities below the salt. Figure 10-42 and Figure 10-43 illustrate this. Figure 10-42(a) through (k) graphically depict the utilization of what might be called estimated velocities in (a) and (b) through constant velocity increases from 5,000 ft/sec through 7,000 ft/sec in (c) through (l). Similarly Figure 10-43(a) through (l) depict the utilization of velocities ranging from 7,500 ft/sec through 10,000 ft/sec.

Figure 10-42. SEG AA′ Second Iteration Autopicked Models and Sections Using Increasing Velocities Below Salt

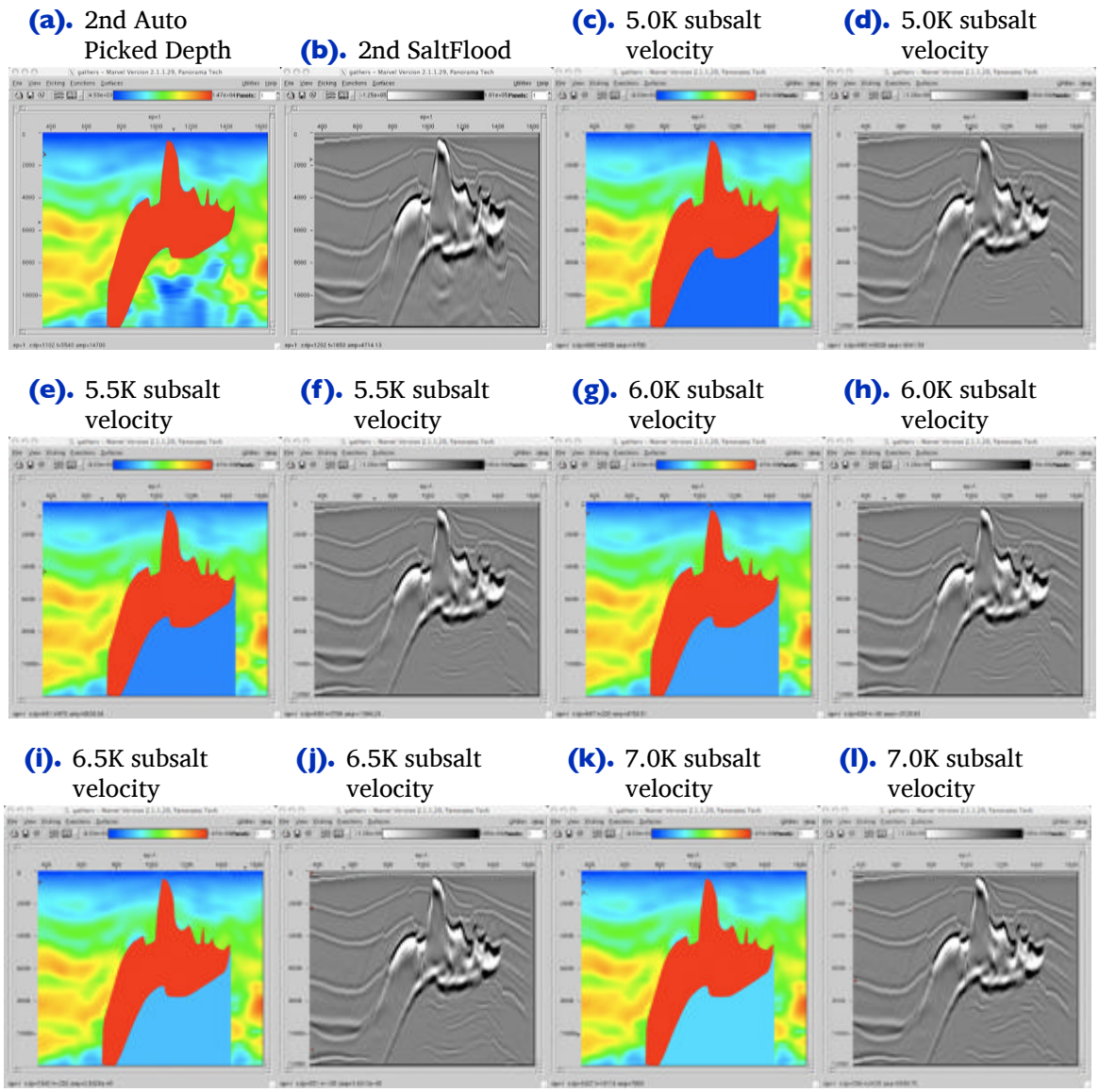

Figure 10-43. SEG AA′ Second Iteration Autopicked Models and Sections using increasing velocities below salt

(a). 7.5K subsalt velocityl **(b).** 7.5K subsalt velocity **(c).** 8.0K subsalt velocity **(d).** 8.0K subsalt velocity

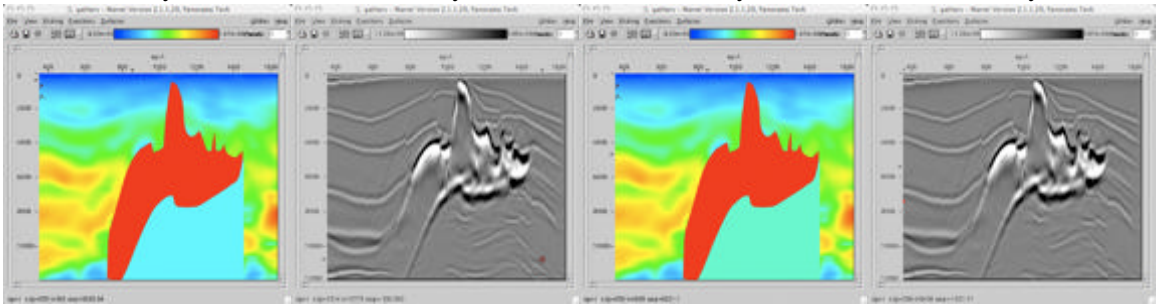

(e). 8.5K subsalt velocity **(f).** 8.5K subsalt velocity **(g).** 9.0K subsalt velocityl **(h).** 9.0K subsalt velocity

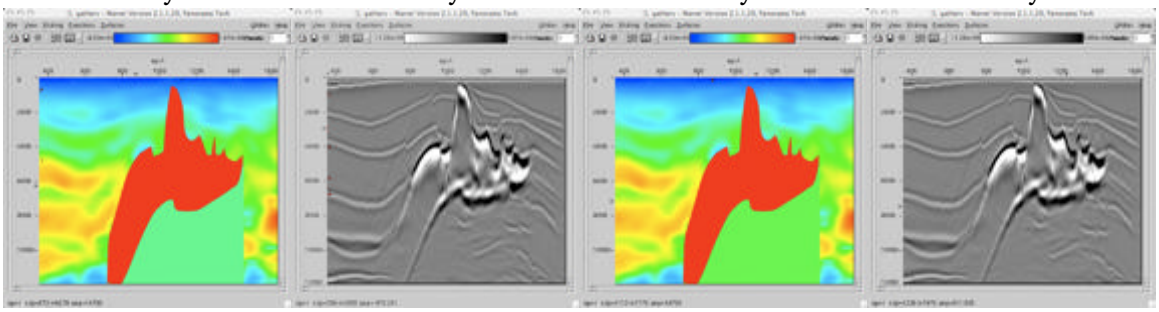

(i). 9.5K subsalt velocity **(j).** 9.5K subsalt velocity **(k).** 10K subsalt velocity **(l).** 10K subsalt velocityt

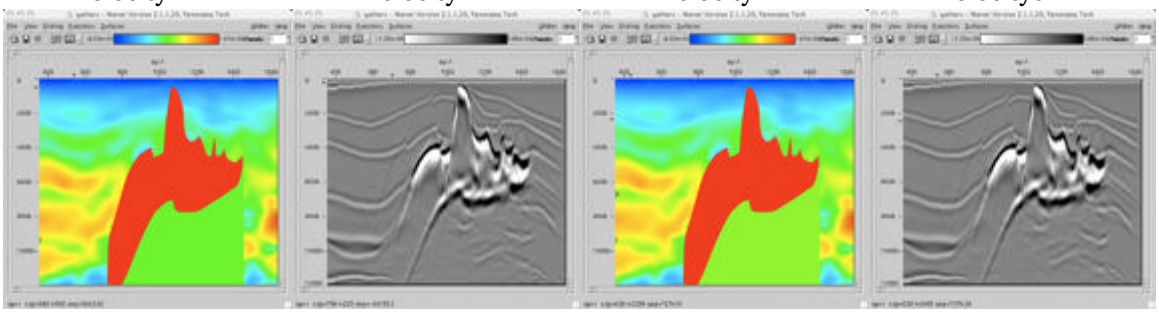

After Tomography

A careful analysis of the migration images in Figure 10-42 and Figure 10-43 suggests that the closest correct sub-salt velocity is about 9,000 ft/sec. Based on this assumption, the input data were re-migrated using 9,000 ft/sec below salt velocity and a dip-based-automatic-flattening analysis performed to generated the necessary input for residual tomography. Residual tomography was then applied to generate a new model and the data re-migrated. Figure 10-44(a) displays the tomographically-estimated velocity while (b) shows the true velocity model.

Figure 10-44. Estimated versus True Velocity model.

(a). Estimated Velocity Model **(b).** True Velocity Model

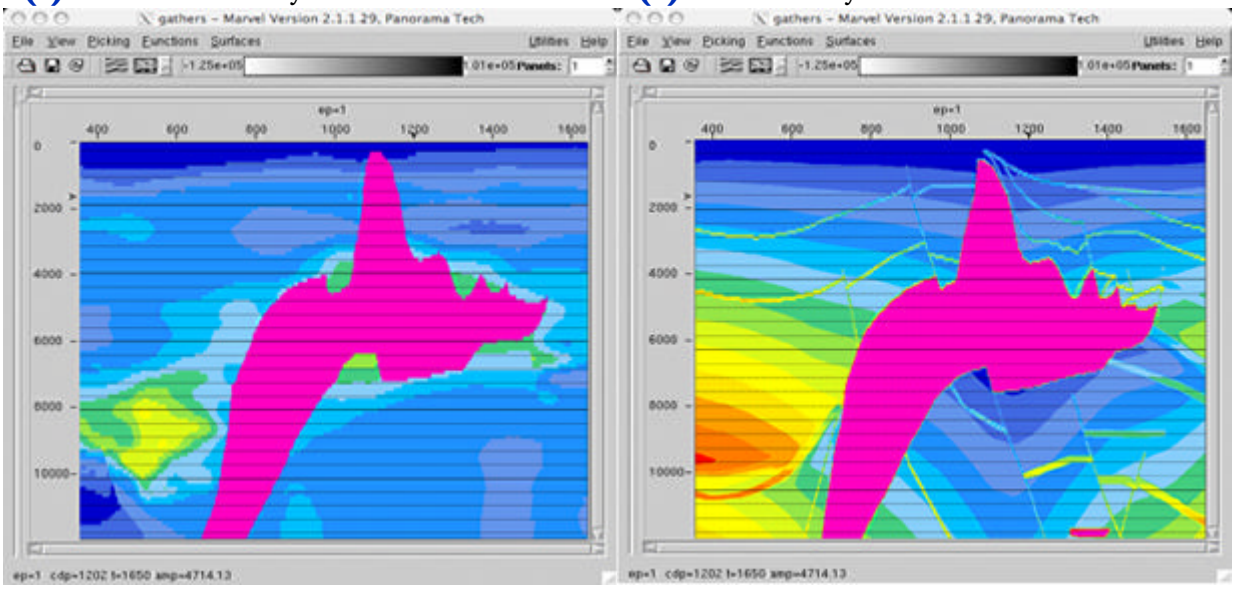

The flatness of the after-tomography gathers is illustrated in Figure 10-45(a) and (b). The gathers in Figure 10-45(a) figure are within what might be called sedimentary geology, while those in part (b) fall within the salt regime.

Figure 10-45. Gathers after Tomography

(a). After Tomography in Sediments **(b).** After Tomography in Salt

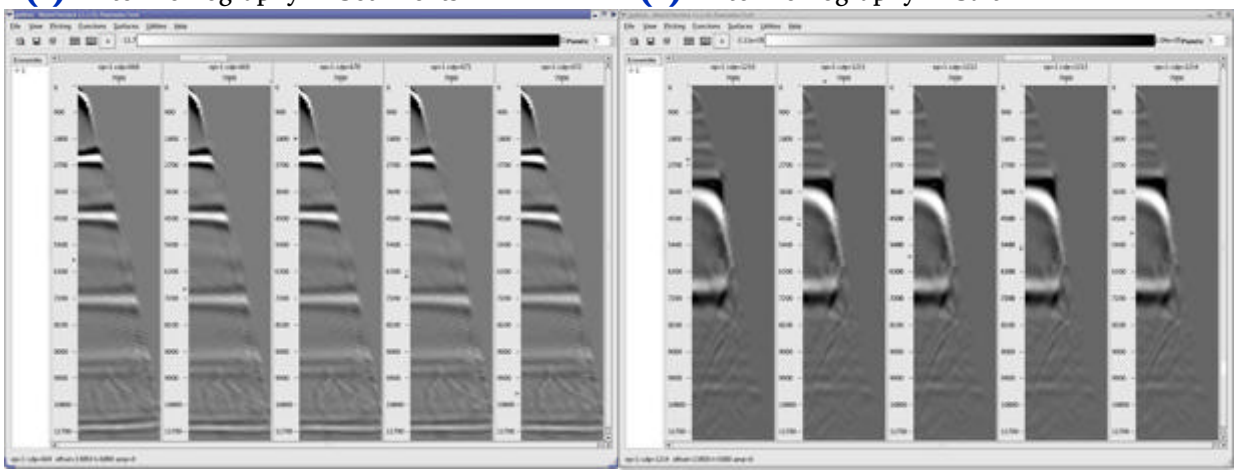

Figure 10-46 is a full comparison between utilization of the estimated velocity field in Figure 10-44(a) and the exact velocity field in (b). Note that in every case the one-way algorithm has produced an image that is significantly better than its Kirchhoff counterpart.

Figure 10-46. Estimated versus True Velocity Image Comparisons.

(a). Kirchhoff using Estimated Model

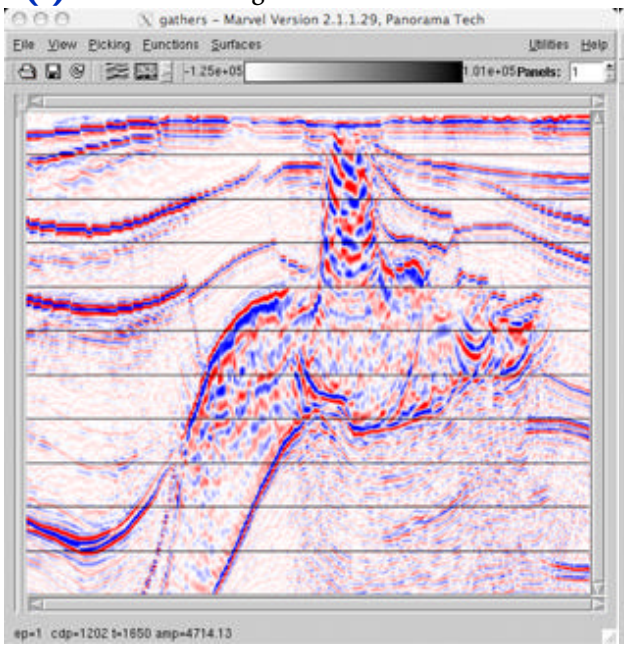

(b). Kirchhoff using Exact Model

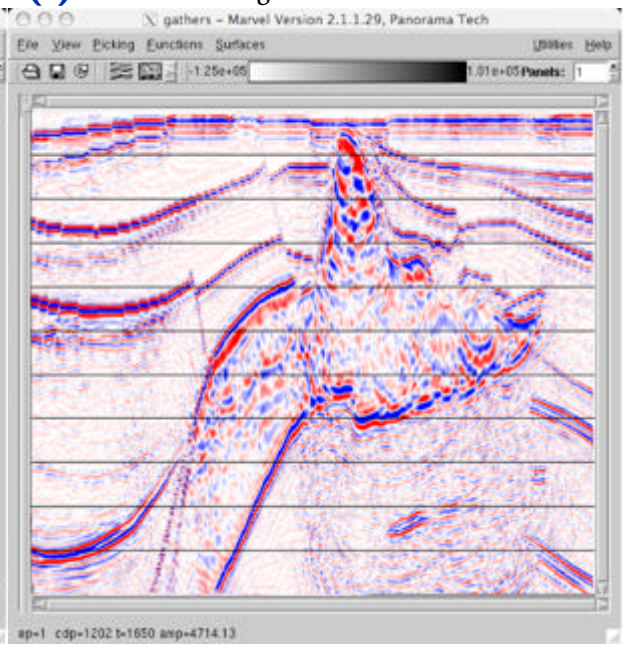

(c). One Way using Estimated Model

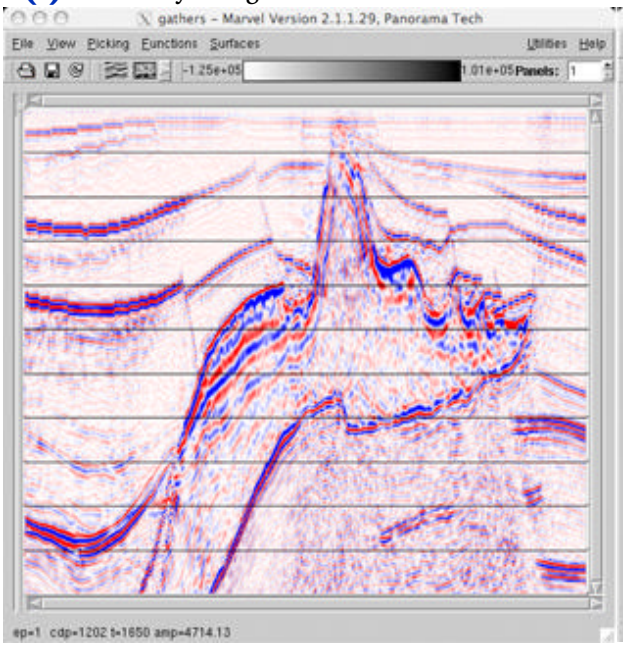

(d). One Way using Exact Model

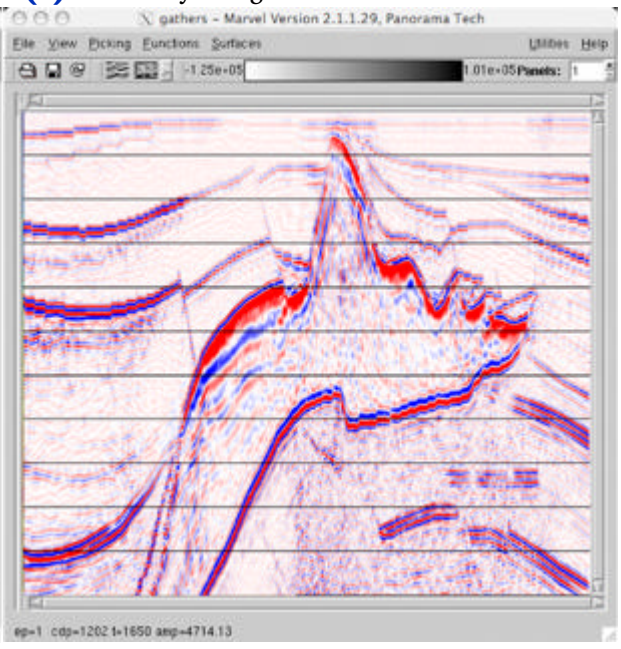

Marmousi Case Study

The original Marmousi data set is somewhat of an enigma. It was designed based on offshore Angola geology and represents a double anticline with the upper anticline sitting virtually directly on top of the lower. The lower structure was prospective but very difficult to image. Neither prestack time migrations or early depth migrations of the day could successfully image the reservoir. Because of this difficulty, Institute Francais de Petrol constructed a model closely resembling the interpreted structure, shot synthetic data over the model and then presented the data to the geophysical community of the day with a challenge to figure out the model from the data alone.

The synthetic data consisted of 240 96 channel shots spaced at 75 meters. The 96 receivers were separated by 25 meters at an offset 200 meters from the shot. Each receiver was the result of summing a more finely sampled array. The wavelet used in this case was neither minimum, maximum, nor zero delay, but produced an effective delay of about 60 ms in the synthesized data. The challenge thus included wavelet processing as well as velocity analysis or inversion and imaging. The goal was to find the velocity model as accurately as possible.

A paper in the 1990's by Sebastian Geoltrain and Roloff Versteeg suggested that Kirchhoff methods alone could never image this structure. While apparently true at the time, as we saw in the chapter on prestack algorithm examples, the real reason this hypothesis made sense was more closely related to the acquisition parameters than to the imaging algorithm.

Our goal here is to see just haw far we can go to produce something close to the actual true velocity. In this sense, we intend to use every available trick in order to achieve our goal

Figure 10-47 shows typical MVA panels based on the initial stacking velocity analysis shown in Figure 10-48. Of interest are that

- the stacking velocity model in (a) is extremely smooth
- the Dix depth-interval model in (b) is close to a $v(z)$
- the image in (c) is essentially what you get doing a PSTM

The smoothness in this case is directly related to the fact that picking was performed on every 100th CDP and that a rather long smoother was applied during the construction of the full model.

Figure 10-47. Marmousi velocity analysis and NMO CDP 1000.

(a). Marmousi CDP 1000l

(b). Marmousi CDP 1000 Semblance

(c). Marmousi CDP 1000 NMO

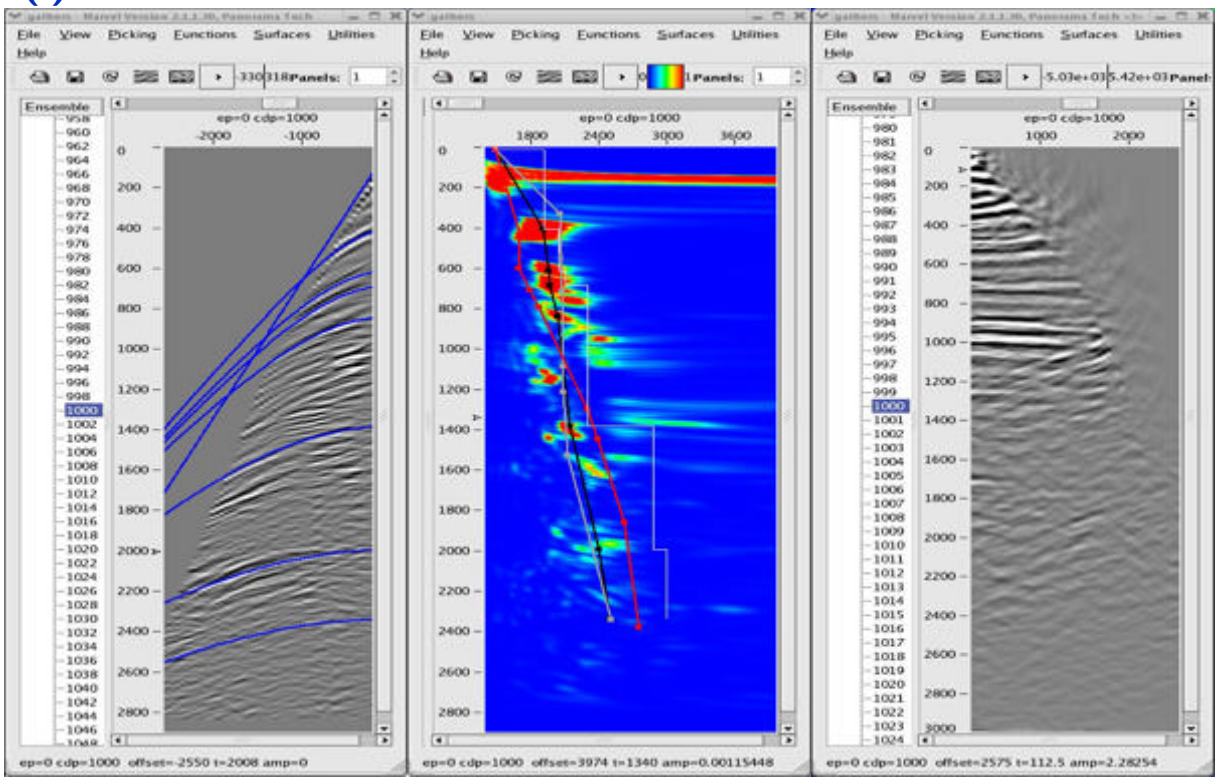

Figure 10-48. Initial Marmousi stacking velocity models and migration.

(a). Stacking Velocity Model

(b). Dix Depth-Interval Model

(c). Migration with (b)

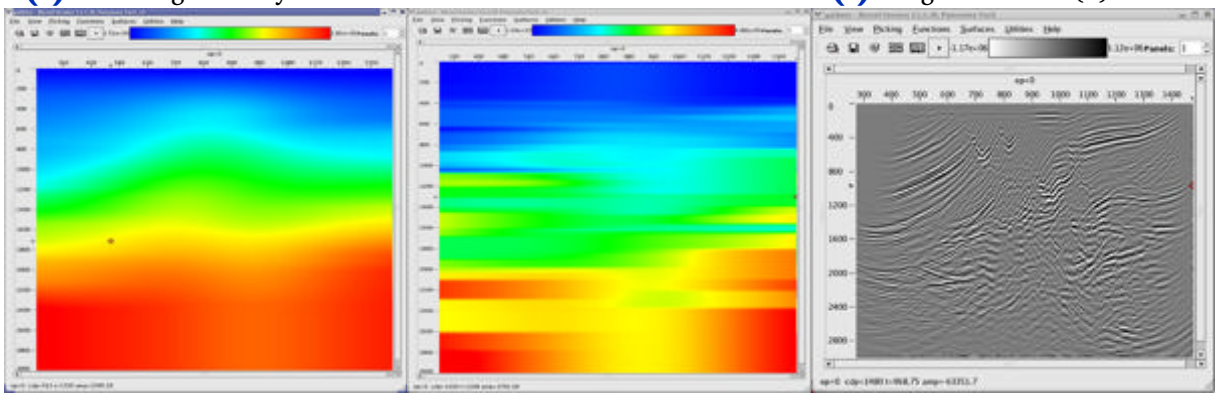

The panels in Figure 10-47 were used to construct the model in Figure 10-49. While the changes are not dramatic, it is clear from the depth-interval model in (b) that the geology does not really follow a $v(z)$ assumption. Note that the image in (c) is also much

more realistic. The only issue in the picking process relates to whether the clear speed up on the left hand side of the model is real or not.

Figure 10-49. Iteration 1 RMS and interval velocity models together with migration based on (b).

(a). Kirchhoff MVA RMS model

(b). Kirchhoff MVA interval velocity modell

(c). First iteration image with (b)

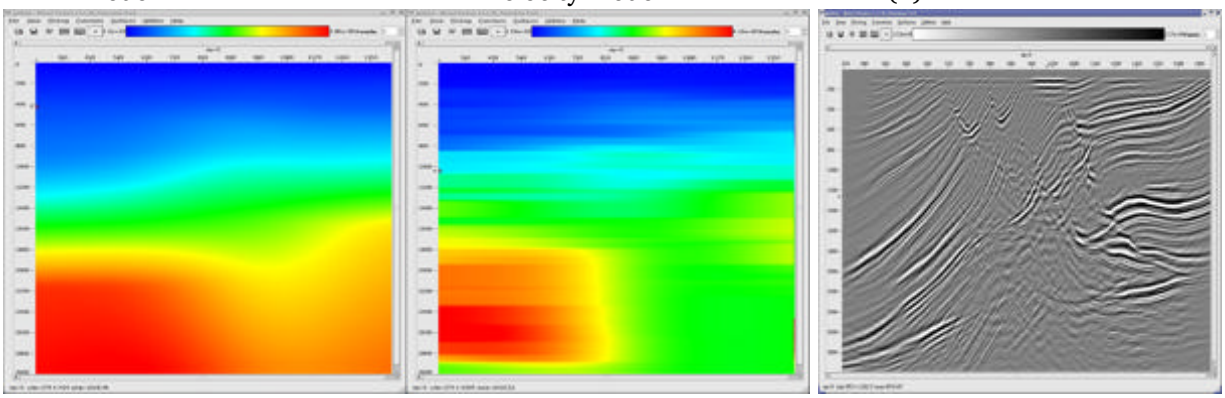

Using the model in Figure 10-49 as a guide, a new model was constructed from the current prestack data to effect a slow down of the left hand side high velocity zone. The result is shown in Figure 10-50(b). Note also that the image is now somewhat more realistic, but the gathers are still not completely flat.

Figure 10-50. First iteration velocity model slowdown together with migration based on (b).

(a). Kirchhoff MVA Interval velocity model

(b). Kirchhoff MVA Slowdown of (a)

(c). First iteration slowdown (b)

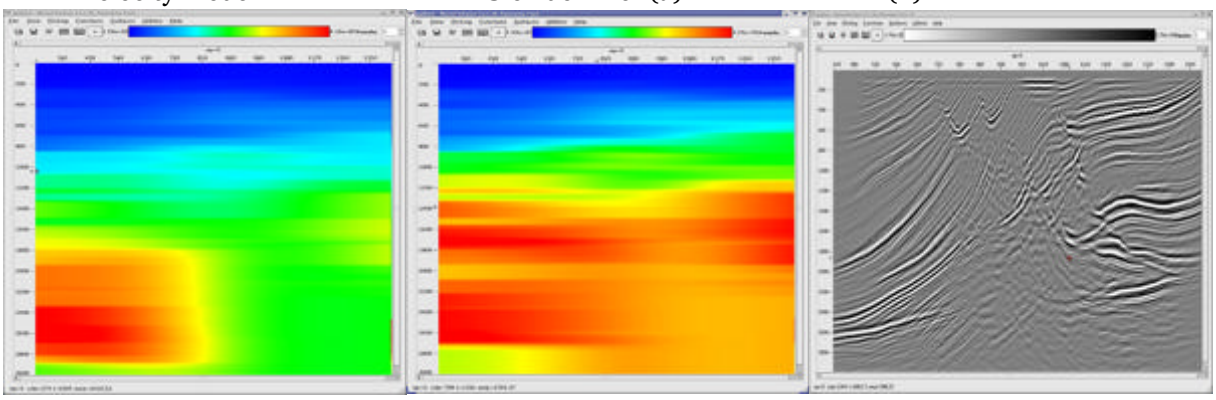

Using the data from the PSDM based on the model in Figure 10-50, panels like those in Figure 10-51 were picked and used to produce the model in Figure 10-52(a) and the migrated image in Figure 10-52(b). When compared to some of the best images produced in the original Marmousi velocity estimate exercise, this image is not too

bad. What is clear is that to improve the answer, several additional iterations will be necessary, but there is absolutely no guarantee that better results will be obtained. In fact, with a nominal maximum offset of just 2600 meters, it is unlikely that velocities below about 1,300 meters per second can be improved much at all.

Is it time to change gears?

Figure 10-51. Marmousi CDP 875 after inverse NMO using the model in Figure 10-50.

(a). Marmousi CDP 875 Semblance **(b).** Marmousi CDP 875

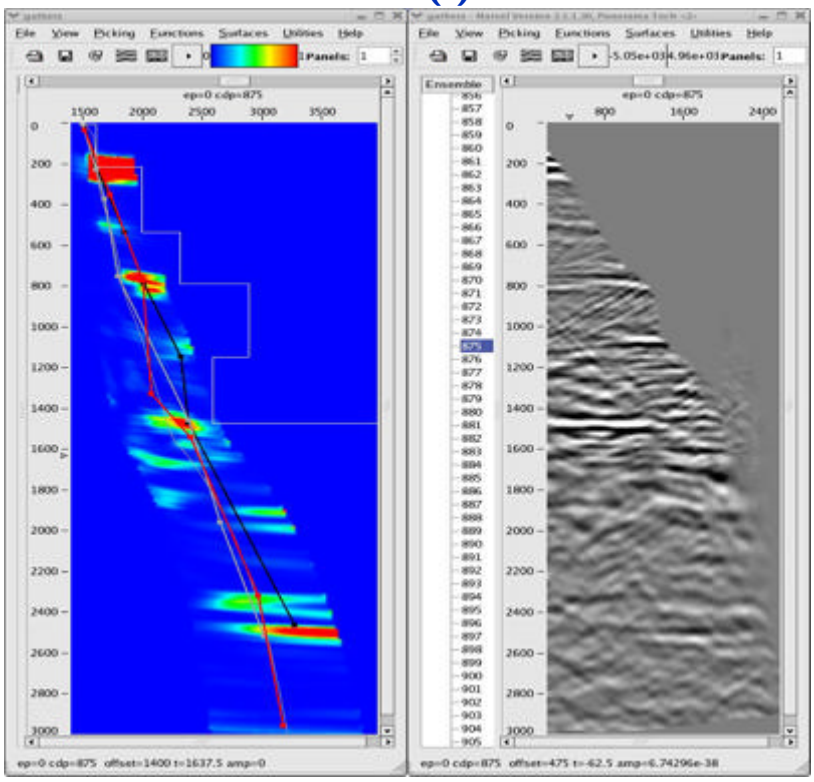

Figure 10-52. MVA Velocity model from migration based on Figure 10-50 model together with migration. In this case, picking was done every 25 CDPs between CDPs 700 and 1200.

(a). MVA Velocity Model **(b).** Migration with MVA model

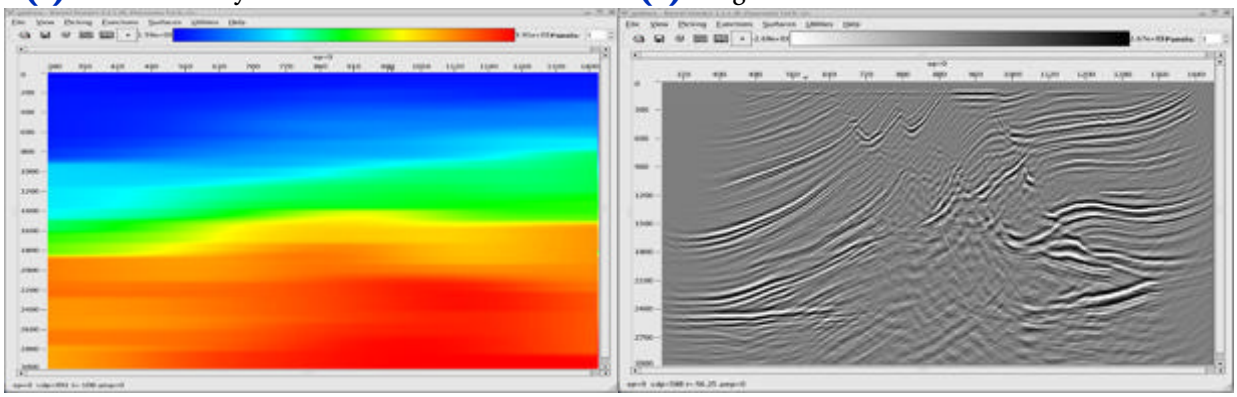

Inversion

At this point in any project, we have a velocity model and an image, but we have no idea how accurate the model is. Realistically, we have more velocity models than we know what to do with, and we don't have a clue as to which one is best.

We also have modeling algorithms, so if we believe our model is so good, why don't we test it by shooting data over the model and subtracting the synthetic from the observed data? That is, for each trace in the observed data, generate a synthetic trace, and then create a completely new data set using a trace-by-trace subtraction. If the model is perfect, we get nothing better than completely random noise and we simultaneously validate the model.

But what if we don't get random noise? Is there any way to use the information from the residual to estimate a new velocity model? The answer is yes, of course, and the mathematical recipe is relatively simple. All we have to do is prestack-reverse-time migrate the difference, normalize in the proper manner and add the result back to the current model. Given the new model, we repeat the process of synthetic generation and subtracting. If the new difference is still not zero, we repeat the exercise until the residual can no longer be reduced. This inversion approach was first presented in the geophysical literature by Lailly in 1983, and Tarantola in 1984. When they tested it, it failed rather miserably. We should not let that bother us. The idea looks sound. Maybe they did something wrong, or maybe they just did not have the computer power to test the theory in an optimum manner. Let us do our own test.

Figure 10-53 shows the result of testing the theory on synthetic data from the Marmousi model. Starting with the $v(z)$ model in (b) of this figure, we synthesized a survey with the same geometry as the data over the model in (a). We then ran the process described

above iteratively. The result after 100 iterations is shown in Figure 10-53(c), and after slightly more than 600 iterations, in (d). Note that the process has worked extremely well. The velocity error in Figure 10-53(e) is virtually zero, except for those areas outside a offset dependent cone. Note also that the RMS error in (f) has been reduced to a very low level. It is probable that we could have stopped after 300 iterations or so, but we cannot argue with the overall results.

Figure 10-53. Marmousi Full Waveform Inversion

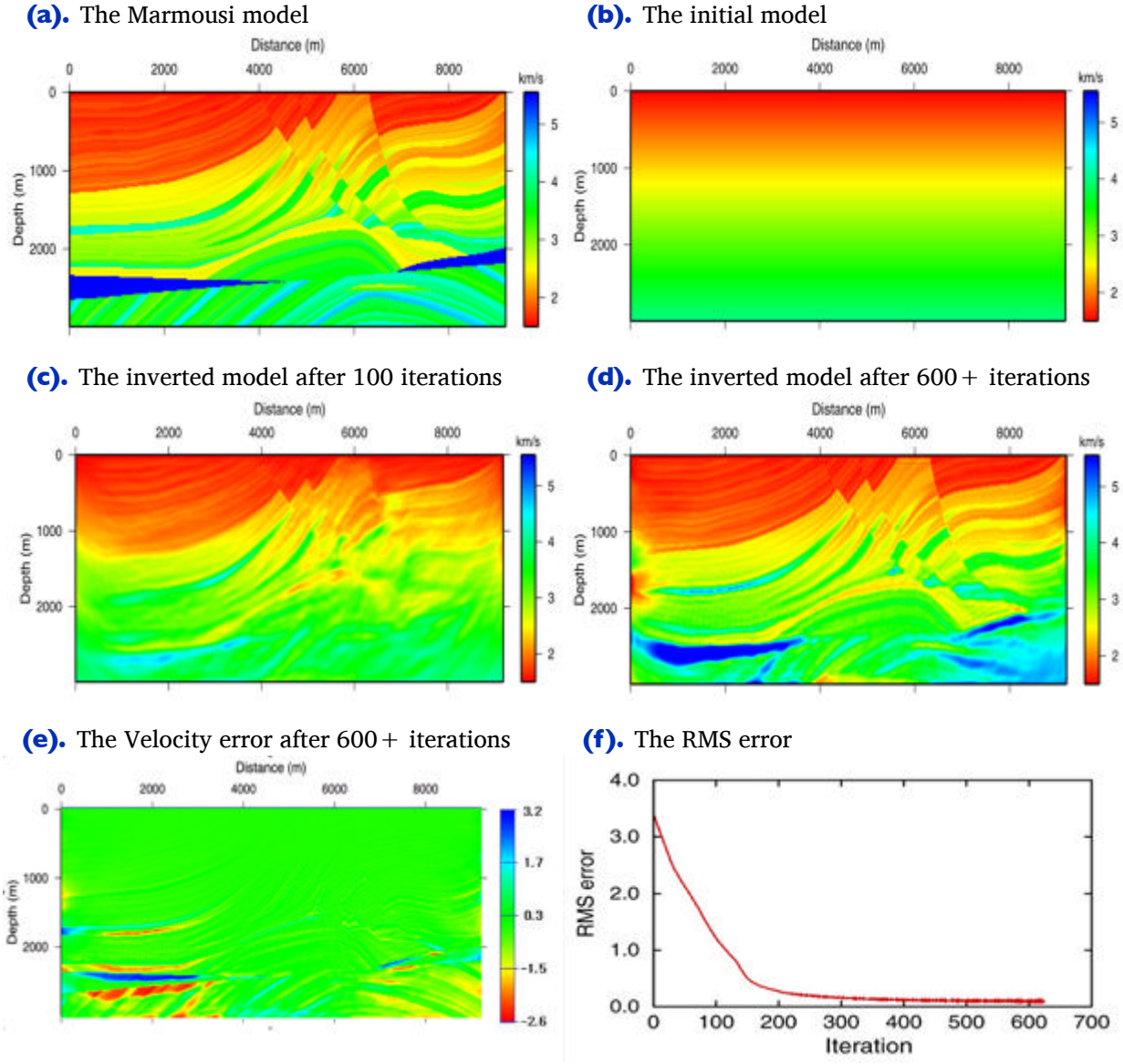

Figure 10-54 further confirms the high quality of the inversion process. This figure shows logs taken at distances of 3000 and 7000 meters from the left hand side of the model. The green line in this figure shows the initial $v(z)$ used to start the process, the red line is the true velocity while the blue line is the inverted velocity after 600+ iterations. Note that down to about 1500 meters, the results are truly outstanding.

Figure 10-54. Inverted Versus True Logs

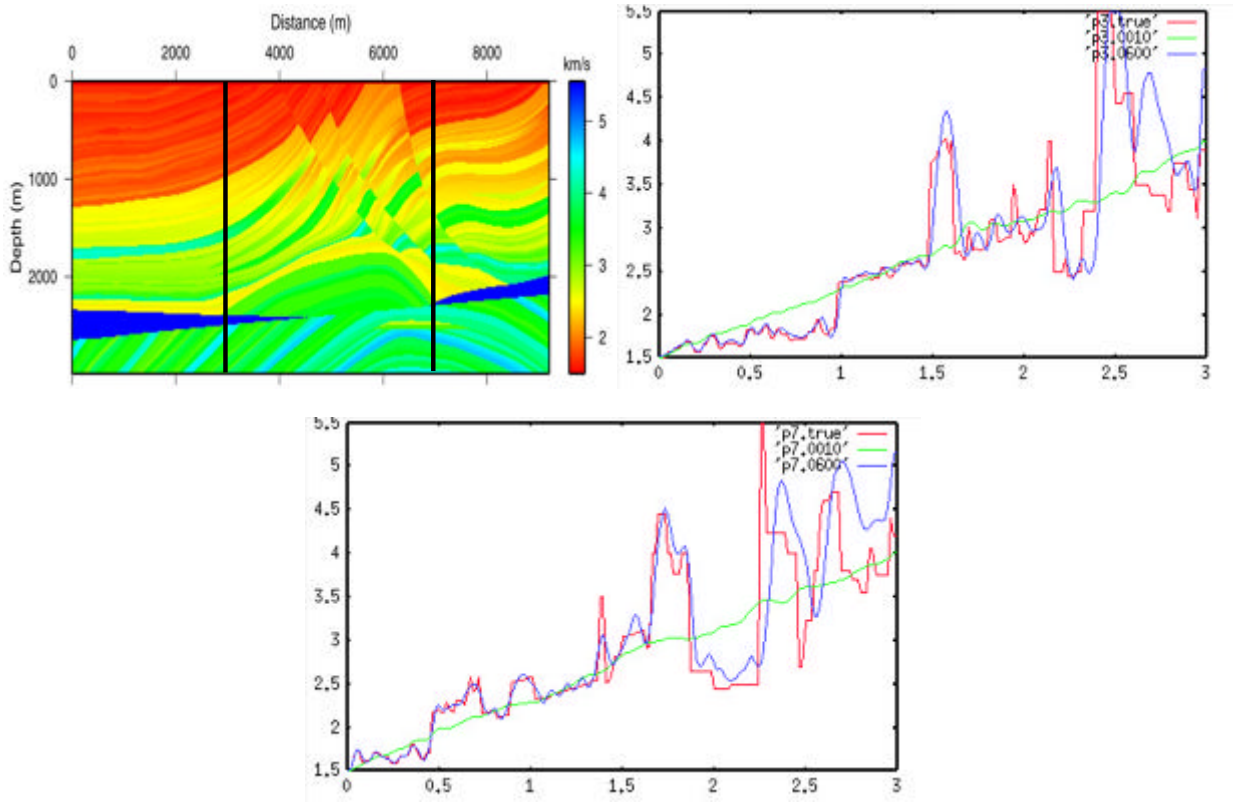

So why did this work now, when it failed so miserably before? Well, to tell the absolute truth, we actually ran the process on extremely low frequency data that we generated over the model in Figure 10-53(a). These data, shown in Figure 10-55, extended over the entire length of the model and had a bandwidth that extended from 0.3 Hz to 18.0 Hz. The model was sampled with a very fine grid to minimize dispersion and to ensure that each modeling exercise was as accurate as possible. However, there is no doubt that the real reason this process worked is directly related to the low frequency content of the data.

Figure 10-55. Marmousi Ultra Low Frequency Synthetic Data